

Low-Energy Universality in Atomic and Nuclear Physics

Lucas Platter

Department of Physics, Ohio State University, Columbus, OH 43210, USA

Abstract. An effective field theory developed for systems interacting through short-range interactions can be applied to systems of cold atoms with a large scattering length and to nucleons at low energies. It is therefore the ideal tool to analyze the universal properties associated with the Efimov effect in three- and four-body systems. In this *progress report*, we will discuss recent results obtained within this framework and report on progress regarding the inclusion of higher order corrections associated with the finite range of the underlying interaction.

Contents

1	Introduction	3
2	Effective Field Theories	4
2.1	The Effective Range Expansion	5
2.2	The Short-Range EFT	6
2.3	The Three-Body System	8
2.4	The Four-Body System	17
3	Low-Energy Universality in Atomic Physics	20
3.1	Three-Body Recombination of Identical Bosons	22
3.2	Three-Body Recombination of Fermions	27
3.3	Atom-Dimer Relaxation	29
3.4	Four-Body Recombination	31
3.5	Challenges and Opportunities I	32
4	Low-Energy Universality in Nuclear Physics	32
4.1	Two Nucleons	33
4.2	Three Nucleons	34
4.3	Four and more Nucleons	38
4.4	Halo Nuclei	39
4.5	Challenges and Opportunities II	41
5	Final Words	41

1 Introduction

Universal properties are one reason why few-body systems with a large scattering length a have received a lot of attention lately. For example, a two-body system with a large positive scattering length a has a bound state with binding energy

$$E_D = \frac{1}{ma^2}, \quad (1)$$

where m denotes the mass of the particles (note that we set $\hbar = 1$ for convenience). In the three-body sector a large two-body scattering length leads to further universal features known widely as Efimov physics [1]. These are fascinating and exciting since they relate physical effects that occur at very different length scales. In experiments with ultracold atoms Feshbach resonances allow the interatom scattering length to be tuned from $-\infty$ to ∞ , while also the internucleon interaction exhibits a scattering length large compared to the range of the interaction.

An understanding of such systems improves therefore also our understanding of low-energy nuclear physics. Moreover, a simple approach only in terms of the large scattering and the other remaining low-energy parameters of the effective range expansion grants also the possibility to address important problems in nuclear few-body systems in a very effective manner. One prominent example is the model-independent description of electroweak reactions relevant to nuclear astrophysics. An approach whose parameters are only related to the effective range expansion might seem inappropriate for such nuclear reactions but it is important to realize that many important processes occur at energies well below the energy scale set by the range of the interaction (i.e. the pion mass m_π).

Since such an approach will fail for observables for which the pion-exchange character of the internucleon interaction is important, it can therefore also answer the question for which measurable quantities the chiral character of the nucleon-nucleon interaction is relevant. This addresses the question what low-energy information in particular is required to describe nuclear systems at different energy scales.

The framework that we will use to address processes in such systems is that of effective field theory (EFT). It allows to obtain model-independent results in a small parameter expansion. The advantages of a calculation of observables in the EFT framework are numerous. Firstly, it allows for a clear separation of the unknown ultraviolet and known low-energy physics which eliminates any possible model-dependence. Secondly, the accuracy of calculated observables can be systematically improved by calculation of another order in the low-energy expansion. And thirdly, the quantum field-theoretic setup brings along the advantages of mathematically tools successfully used in high-energy physics, such as Feynman diagrams, renormalization and regularization.

Here we will concentrate on applications of one particular EFT (that we will call *short-range EFT*) that is tailored to the problem of short-range interactions. The expansion parameters in this EFT are R/a and kR , where R denotes the range of the underlying interaction and k the momentum scale of the process under consideration. At leading order, this EFT framework allows us to analyze the

properties of systems interacting through zero-range interactions. Finite range effects can then be accounted for by calculating subleading orders in the EFT expansion.

The short-range EFT provides therefore a good framework to analyze the few-body dynamics in resonantly interacting ultracold gases. Binding energies and scattering observables can be calculated and the experimental signals of Efimov physics can therefore be identified.

Predictions for low-energy scattering processes and binding energies can also be made in the nuclear case. However, the field-theoretic formulation of this framework facilitates in addition a calculation of electroweak observables relevant to nuclear astrophysics as discussed above.

The purpose of this review is to display the similarities between low-energy atomic and nuclear physics and to demonstrate that the same framework can be applied to both sectors to obtain relevant and interesting results. In contradistinction to recent reviews on similar topics [2, 3, 4, 5], we will present the applications and results for atomic and nuclear systems alongside. By doing this we want to emphasize the similarities between low-energy nuclear physics and the few-body dynamics in resonantly interacting ultracold gases of alkali atoms.

We will be mainly interested in few-body systems and will therefore mainly focus on systems that can be described either as two, three or four-body systems. It should also be noted that this is not a complete review of work done for systems with short-range interactions but instead it should be considered as a *progress report* that gives a brief introduction to the short-range EFT, that presents recent calculations performed in the few-body sector and discusses then an incomplete list of problems that should be addressed in the near future.

In the following chapter, we will thus give a brief introduction to the concept of EFTs and will discuss in detail the short-range EFT whose application to different problems will be covered in the remaining sections of this review. In section 3, we will give a review of recent applications of the short-range EFT to systems of ultracold atoms. In section 4 we will review results obtained with short-range EFT for nuclear systems such as the three- and four-nucleon systems but also heavier systems such as halo nuclei. We will conclude with a summary.

2 Effective Field Theories

Effective field theories are an excellent tool to describe the interactions in systems with a separation of scales. The usual example of such a scale separation is the ratio of a small momentum over a heavy mass scale. The weak interaction for example, can be described without explicit use of heavy vector bosons if the energies of the processes are well below the mass scale of the exchange particles. In this case the weak interactions can be described very well with the familiar Fermi interaction.

Here, we will focus on the short-range EFT, which is tailored to describe non-relativistic particles with a large scattering length a at low energies. We will discuss the Lagrangian which is at the heart of the EFT and describe how it can be used along with an ordering scheme called power counting and Feynman rules

to obtain a powerful framework for the computation of low-energy observables of few-body systems with a large two-body scattering length.

Very good introductions to the general concepts of EFTs have been written by Kaplan [6], Lepage [7] and Polchinski [8]. An excellent introduction to EFTs applied to nuclear systems has been given by Phillips [9].

2.1 The Effective Range Expansion

We will consider identical particles (bosons for simplicity) interacting via a potential that has a finite range R . In this case the amplitude for the scattering of two particles can be written as

$$\mathcal{A}(k, \cos \theta) = \frac{8\pi}{m} \sum_l \frac{2l+1}{k \cot \delta_l - ik} P_l(\cos \theta) , \quad (2)$$

where k denotes the relative momentum between the two particles, m is the mass of each of these particles and δ_l denotes the scattering phase shift in partial wave l .

At low momenta, the expression in the denominator can be expanded in even powers of the momentum k

$$k^{2l+1} \cot \delta_l = -\frac{1}{a_l} + \frac{r_l}{2} k^2 + \mathcal{O}(k^4) . \quad (3)$$

For the S - and P -wave phase shifts, the first terms in the expansions are

$$k \cot \delta_0 = -\frac{1}{a} + \frac{1}{2} r_s k^2 + \dots , \quad k \cot \delta_1 = -\frac{3}{k^2 a_p^3} + \dots , \quad (4)$$

where a , a_p are the S - and P -wave scattering lengths, respectively, r_s is the S -wave effective range and the ellipses denote higher order terms in the expansion.

For large positive scattering length, one finds a bound state as discussed above and we will frequently use the effective range expansion (ERE) around the bound state pole:

$$k \cot \delta_0 = -\gamma + \frac{\rho}{2} (\gamma^2 + k^2) + \dots , \quad (5)$$

where $E_D = \gamma^2/m$ and $\rho = r_s$ up to the orders considered in this work.

The low-energy physics encoded in the effective range parameters depends on the relative size of these parameters. In the following we will consider two special cases which we will refer to as the *natural case* and the *unnatural case*. In the natural case, all effective range parameters are of natural size, i.e. of the order of the range of the interaction $a \sim r_s \sim R$. In this case the scattering amplitude in Eq. (2) can be expanded in powers of k :

$$\mathcal{A}(k) = -\frac{8\pi a_s}{m} [1 - ia_s k + (a_s r_s / 2 - a_s^2) k^2 + \dots] . \quad (6)$$

For simplicity we have considered here only the S -wave projected part of the scattering amplitude. This expansion will converge for momenta $k \ll 1/R$.

Now consider the case in which the scattering length a is much larger than all other effective range parameters $|a| \gg |r_s| \sim R$. This separation of scales indicates the presence of non-perturbative physics through a (virtual) bound state with energy $\sim 1/(ma^2)$. The expansion above is only valid for $ak \ll 1$ which reduces the radius of convergence dramatically and renders it useless in the limit of infinite scattering length. We will instead expand in powers of kR and keep ak to all orders:

$$\mathcal{A}(k) = -\frac{8\pi}{m} \frac{1}{1/a + ik} \left[1 + \frac{r_s/2}{1/a + ik} k^2 + \frac{(r_s/2)^2}{(1/a + ik)^2} k^4 + \dots \right]. \quad (7)$$

The resulting expansion still converges for $kR \ll 1$ and reflects the fact that systems with a large two-body scattering length require a non-perturbative resummation at *leading order*.

2.2 The Short-Range EFT

Our goal is to describe the dynamics of particles interacting through a short-range potential with an EFT. The Lagrange density for an EFT is generated by writing down all possible operators built from the available degrees of freedom in accordance with the required symmetries. At sufficiently low momenta, non-relativistic particles can be described by an EFT built up from contact interactions alone. This EFT can be applied if the relative momenta k of the particles is much smaller than the inverse of the range of the underlying interaction R :

$$k \ll 1/R. \quad (8)$$

The convergence radius of our EFT will therefore agree with that of the ERE and we can therefore anticipate that we will be able fix any free parameters in the two-body sector from the ERE.

The only degrees of freedom we require for our EFT are therefore the atoms themselves. Having identified the relevant degrees of freedom, we generate the effective Lagrangian by writing down all possible operators satisfying the constraints of Galilean, parity and time-reversal invariance and locality:

$$\mathcal{L} = \psi^\dagger \left[i\partial_t + \frac{\nabla^2}{2m} \right] \psi - \frac{C_0}{4} (\psi^\dagger \psi)^2 - \frac{D_0}{36} (\psi^\dagger \psi)^3 - \frac{E_0}{576} (\psi^\dagger \psi)^4 \dots,$$

The ellipses represent operators of higher dimension which means terms with more derivatives and/or more fields. We have neglected relativistic effects which are suppressed by factors of $(p/M)^2$. D_0 and E_0 denote the leading three- and four-body interactions.

Every EFT contains therefore an infinite number of two- and many-body operators. This framework might therefore seem useless since an infinite number of Feynman diagrams arises for every observable and infinite number of coupling constants needs to be determined from experiment. Here, the afore-mentioned separation of scales allows us to resolve this problem. The separation of scales usually leads to a ratio of a light scale over a heavy scale (e.g. a small momentum divided by a large mass) which is exploited as a small expansion parameter α_{EFT} .

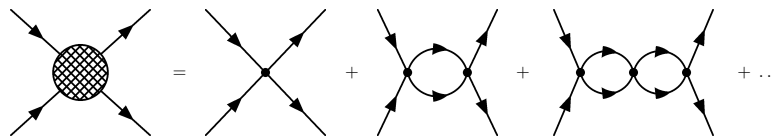


Figure 1. The sum of diagrams including the C_0 vertex contributing to two-body scattering.

Appropriate renormalization of the vertex constants (also known as low-energy constants) will then lead to an ordering of all possible Feynman diagrams (power counting) such that only a well-defined number of low-energy constants are required at each order of the expansion of a matrix element in powers of α_{EFT} . This power counting arises in the short-range EFT by demanding that the scattering amplitude for two-body scattering reproduces the appropriate momentum expansion (Eqs. (6) and (7)) of the scattering amplitude.

Feynman rules:

As in standard quantum field theory, amplitudes for processes are calculated by using Feynman rules derived from the Lagrange density. The Feynman rules for the short-range EFT are particularly simple

- Assign non-relativistic four-momenta (p_0, \mathbf{p}) to all lines and enforce momentum conservation at each vertex.
- For each vertex include a factor $-i$ times the low-energy constant of the corresponding operator.
- For each internal line include the propagator with four-momentum (p_0, \mathbf{p})

$$iS(\mathbf{q}, q_0) = \frac{i}{q_0 - \frac{q^2}{2m} + i\epsilon}, \quad (9)$$

- Integrate over all undetermined loop momentum using the measure

$$\int \frac{dq_0}{2\pi} \frac{d^3q}{(2\pi)^3}.$$

The energy integral can be evaluated using contour integration.

- Multiply by a symmetry factor $1/n!$ if the diagram is invariant under the permutation of n internal lines.

Power counting

It is clear from the discussion on the expansion of the two-body amplitude for large scattering length that the power counting requires a resummation of an infinite set of diagrams to obtain the pole structure of Eq. (7). Here, we will verify by explicit calculation that the leading order two-body amplitude can be reproduced by summing up all diagrams including only the C_0 vertex as shown in Fig. 1.

Using the Feynman rules given above, the sum of diagrams shown in Fig. 1 can be expressed as

$$\begin{aligned} \mathcal{A}(E) &= -iC_0 \sum_{n=0}^{\infty} (-iC_0 \mathcal{I}/2)^n \\ &= \frac{-iC_0}{1 + iC_0 \mathcal{I}/2}, \end{aligned} \quad (10)$$

where \mathcal{I} is given by

$$\mathcal{I} = \int \frac{dq_0}{2\pi} \frac{d\mathbf{q}^3}{(2\pi)^3} \frac{i}{p_0 - q_0 - \frac{\mathbf{q}^2}{2m} + i\epsilon} \frac{i}{q_0 - \frac{\mathbf{q}^2}{2m} + i\epsilon} \quad (11)$$

$$= im \left(\frac{\Lambda}{2\pi^2} - \frac{\sqrt{-mp_0}}{4\pi} \right). \quad (12)$$

This integral has been regularized with an ultraviolet cutoff Λ . Inserting Eq. (12) in (10), we end up with the expression

$$\mathcal{A} = \frac{8\pi}{m} \left[-\frac{8\pi}{mC_0} - \frac{2\Lambda}{\pi} + \sqrt{-mp_0} \right]^{-1}. \quad (13)$$

We reproduce the leading order term in Eq.(7) by setting

$$C_0 = \frac{8\pi a}{m} \frac{1}{1 - 2\Lambda a/\pi}. \quad (14)$$

In the two-body system the leading order amplitude is therefore given by the sum of all diagrams which contain only the C_0 vertex. Subleading corrections can then be calculated from perturbative insertions of the higher order operators dressed to all orders by C_0 .

The short-range EFT power counting for the two-body sector was developed in Refs. [10, 11, 12, 13, 14]. A regularization scheme alternative to cutoff regularization which makes the powercounting on a diagram-by-diagram basis explicit was developed in Refs. [11, 12].

It has to be emphasized that the powercounting is of course different in the case of a scattering length of natural size, i.e. $a \sim R$. In this case the powercounting and therefore the order at which a particular diagram contributes follows directly from naive dimensional analysis of the corresponding operators. This EFT is only of limited interest in the few-body sector, but it has found interesting applications in the many-body sector [15, 16].

2.3 The Three-Body System

Applications of the framework laid out above to the two-nucleon system have been very successful (for a review see Ref. [4]).

Bedaque, Hammer and Van Kolck were the first to consider the three-body system using the short-range EFT [17, 18]. They used an equivalent form of the Lagrange density given in Eq. (9) that turns out to simplify the treatment of the



Figure 2. The dressed dimeron propagator

three-body system. This form uses an auxiliary field, the dimeron T , which has the quantum numbers of a two-body state [17]:

$$\mathcal{L} = \psi^\dagger \left(i\partial_t + \frac{\vec{\nabla}^2}{2m} \right) \psi + \Delta T^\dagger T - \frac{g}{\sqrt{2}} (T^\dagger \psi \psi + \text{h.c.}) + h T^\dagger T \psi^\dagger \psi \dots \quad (15)$$

The Lagrange density above is equivalent to the density in Eq. (9) if the low-energy constants are chosen to be $2g^2/\Delta = C_0$ and $-18hg^2/\Delta^2 = D_0$. The dimeron field T has the bare propagator

$$\frac{i}{\Delta}. \quad (16)$$

It is clear that the power counting introduced in the previous section dictates a resummation of the particle-particle loops as shown in Fig. 2. We therefore obtain the *dressed* dimeron propagator ¹:

$$\begin{aligned} iD(p_0, \mathbf{p}) &= \frac{-i}{-\Delta + \frac{mg^2}{4\pi} \sqrt{-mp_0 + \frac{\mathbf{p}^2}{4}} - i\epsilon} \\ &= -\frac{4\pi}{mg^2} \frac{i}{-1/a + \sqrt{-mp_0 + \mathbf{p}^2} - i\epsilon}. \end{aligned} \quad (17)$$

This propagator has a pole at $p_0 = p^2/(4m) - (4\pi\Delta/(mg^2))^2/m$. Evaluating the residue of Eq. (17) leads to the wavefunction renormalization factor

$$Z_D = \frac{8\pi}{m^2 g^2 a}. \quad (18)$$

Let us consider now elastic scattering between an atom and a dimer shown diagrammatically in Fig 3. Using the Feynman rules discussed previously with the added information on the dimeron propagator, we can consider the amplitude for elastic particle-dimer scattering.

$$\begin{aligned} t(\mathbf{p}, \mathbf{k}; E) &= \frac{2mg^2}{k^2 + p^2 + mE + \mathbf{p} \cdot \mathbf{k}} + h \\ + 8\pi \int \frac{d^3q}{(2\pi)^3} \frac{1}{-1/a + \sqrt{3q^2/4 - mE} - i\epsilon} &\left[\frac{t(\mathbf{q}, \mathbf{k}; E)}{-mE + q^2 + p^2 + \mathbf{p} \cdot \mathbf{q}} + \frac{h}{2mg^2} \right]. \end{aligned} \quad (19)$$

The reason why we have included the three-body interaction h will be discussed below.

¹No cutoff dependence appears in the expressions for the two-body propagator in Eq. (17) since we assume that the bubble loop integrals from the two-loop sector were evaluated using dimensional regularization with minimal subtraction.

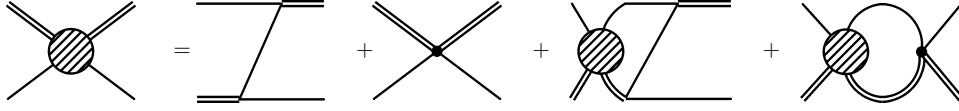


Figure 3. The integral equation for the atom-dimer scattering amplitude t

In order to relate the amplitude to observables, we have to multiply t with the wavefunction renormalization Z_D factor from Eq. (18). It is therefore convenient to rewrite the integral equation:

$$\begin{aligned}
 t_R(\mathbf{p}, \mathbf{k}; E) &= \frac{16\pi}{ma} \left[\frac{1}{k^2 + p^2 - mE + \mathbf{p} \cdot \mathbf{k}} + \frac{H(\Lambda)}{\Lambda^2} \right] \\
 &+ 8\pi \int \frac{d^3q}{(2\pi)^3} \frac{1}{-1/a + \sqrt{3q^2/4 - mE - i\epsilon}} \left[\frac{t_R(\mathbf{q}, \mathbf{k}; E)}{-mE + q^2 + p^2 + \mathbf{p} \cdot \mathbf{q}} + \frac{H(\Lambda)}{\Lambda^2} \right], \quad (20)
 \end{aligned}$$

where $t_R = Z_D t$ and $h = 2mg^2 H(\Lambda)/\Lambda^2$. The total energy in this process is given by $E = \frac{3}{4m} \mathbf{k}^2 - E_D$ and the on-shell point is given by $\mathbf{k} = \mathbf{p}$. It is straightforward to decompose the amplitude into contributions from channels with different orbital angular momentum quantum number l :

$$t_l(p, k; E) = \frac{1}{2} \int_{-1}^1 dx P_l(x) t(\mathbf{p}, \mathbf{k}; E). \quad (21)$$

where $x = \mathbf{p} \cdot \mathbf{k}/(pk)$ and $P_l(x)$ denotes a Legendre polynomial. Projecting onto S -waves ($l = 0$) gives

$$\begin{aligned}
 t_0(p, k; E) &= \frac{8\pi}{ma} \left[\frac{1}{pk} \ln \left(\frac{p^2 + pk + k^2 - mE}{p^2 - pk + k^2 - mE} \right) + \frac{2H(\Lambda)}{\Lambda^2} \right] \\
 &+ \frac{2}{\pi} \int_0^\Lambda dq q^2 \frac{t(q, k; E)}{-1/a + \sqrt{3q^2/4 - mE - i\epsilon}} \\
 &\times \left[\frac{1}{pq} \ln \left(\frac{p^2 + pq + q^2 - mE}{p^2 - pq + q^2 - mE} \right) + \frac{2H(\Lambda)}{\Lambda^2} \right]. \quad (22)
 \end{aligned}$$

Here a cutoff Λ has been introduced to make the integral equation well-defined. Equation (22) is then related to the atom-dimer phase shift via

$$t_0(k, k) = \frac{3\pi}{m} \frac{1}{k \cot \delta_{AD} - ik}. \quad (23)$$

Equation (20) (without the three-body force) is also known as the Skorniakov-Ter-Martirosian (STM) equation, named after the first ones to derive an integral equation interacting through zero-range two-body interactions [19].

Bound states can be found by solving the homogeneous version of the integral equation in Eq. (22). So far we have not explained why we included the three-body force in our *leading order* equation. Naive dimensional analysis by counting

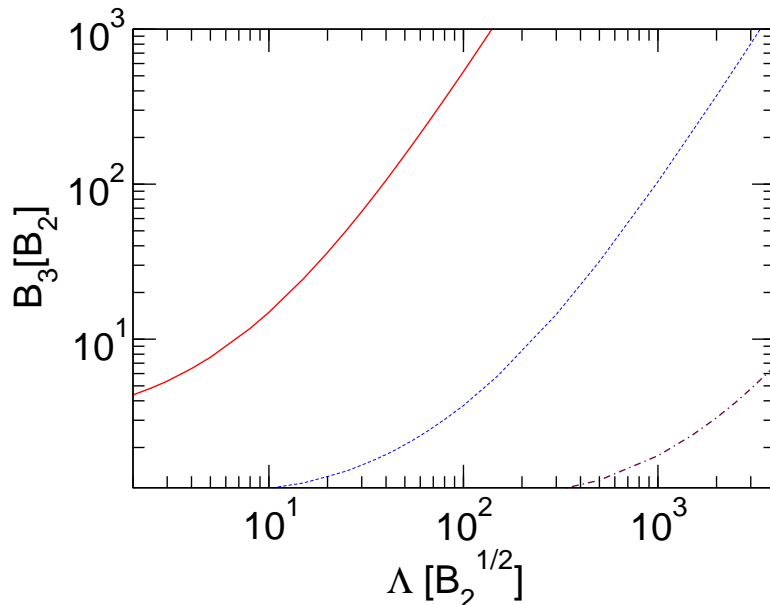


Figure 4. The shallowest three-body binding energies indicated by the solid, dashed, and dash-dotted lines as a function of the momentum cutoff Λ .

the mass dimension of the three-body operator suggests that the three-body force is a higher order effect.

Let us therefore consider the bound state problem and set the three-body force to zero. The resulting strong cutoff-dependence of three-body binding energies is shown in Fig. 4. This cutoff-dependence is no residual dependence which becomes weaker with increasing cutoff but is a genuine result of the use of zero-range interactions in the three-body sector. It was in fact already pointed out by Danilov in the 1960's that the STM equation has no unique solution [20] and it was later suggested by Kharchenko to fix the cutoff and to treat it as a parameter [21]. The field-theoretic perspective implies that three-body observables are sensitive to short-distance effects that have not been properly renormalized.

Bedaque, Hammer and van Kolck [17, 18] showed that the inclusion of the three-body force as in Eq. (22) results in fully renormalized observables². The three-body force $H(\Lambda)$ is therefore included and its value is determined by adjusting Eq. (22) to a given three-body datum (such as the binding energy of a three-body bound state). It was shown furthermore that the cutoff dependence of $H(\Lambda)$ can be approximated with

$$H(\Lambda) = -\frac{\sin(s_0 \ln(\Lambda/L_3) - \arctan(1/s_0))}{\sin(s_0 \ln(\Lambda/L_3) + \arctan(1/s_0))}, \quad (24)$$

²An alternative perspective can be won by an analysis of this problem in coordinate space. An analysis in the hyperspherical formalism shows that the three-body problem with infinite scattering length becomes a Schrödinger like problem with a $1/\mathcal{R}^2$ potential, where \mathcal{R} denotes the three-body hyperradius. The solution to this problem requires a short-distance boundary condition which is determined by a three-body datum. An excellent discussion of the analysis of this problem in the hyperspherical formalism is given in [22].

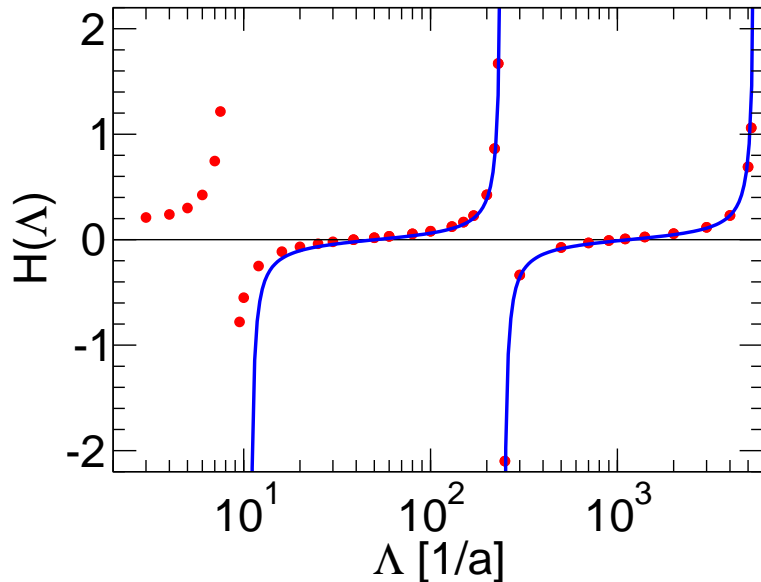


Figure 5. Coupling constant H as a function of the cutoff Λ . The solid shows a fit to Eq. (24) for an arbitrarily chosen three-body renormalization point.

where L_3 is a parameter fixed from experiment and $s_0 \approx 1.00624$. It can easily be seen that $H(\Lambda)$ is periodic in the cutoff. A rescaling of the cutoff Λ by a factor of $\exp(n\pi/s_0) \approx 22.7$ gives back the same result for H

$$H(\Lambda) = H(\Lambda \exp(n\pi/s_0)) . \quad (25)$$

This particular running of the coupling constant H is called a limit cycle and was first discussed as an additional type of renormalization group flow in Ref. [23]. The limit cycle is also reflected in observables: whenever the cutoff is increased by a factor of 22.7, the number of bound states in the spectrum increases by one (as can be seen in Fig. 4). In the limit of infinite scattering length, one finds an infinite tower of three-body bound states:

$$E_T^{(n)} = (e^{-2\pi/s_0})^{n-n_*} \kappa_*^2/m, \quad (26)$$

where κ_* is the binding wavenumber of the Efimov trimer labeled by n_* and m is the mass of the particles. The short-range EFT reproduces therefore at leading order the Efimov effect. Vitaly Efimov discovered in the 1970s that the zero-range limit of the 3-body problem for nonrelativistic particles with short-range interactions shows discrete scale invariance. If $a = \pm\infty$, there are infinitely many 3-body bound states with an accumulation point at the 3-atom scattering threshold. These *Efimov states* or *Efimov trimers* have a geometric spectrum [1]. Furthermore, he pointed out that these results were also valid for finite scattering length as long as $a \gg r_s$. The short-range EFT is therefore an approach in which the properties of few-body systems related to Efimov physics can be analyzed but that furthermore facilitates the systematic inclusion of perturbations due to the finite range of the underlying interaction.

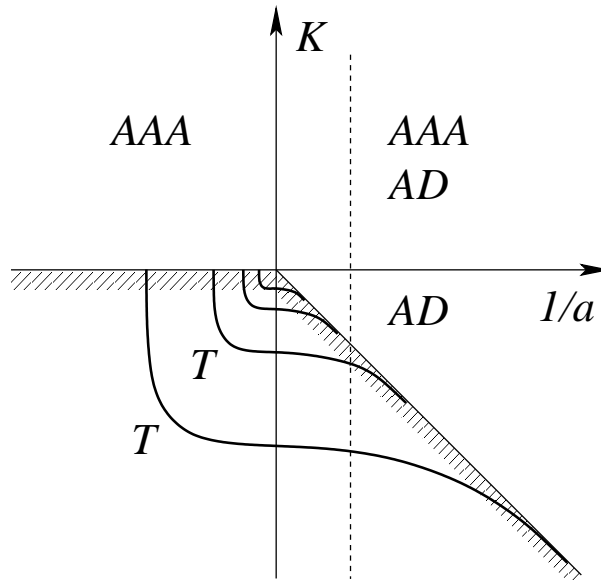


Figure 6. The a^{-1} - K plane for the three-body problem. The allowed regions for three-atom scattering states and atom-dimer scattering states are labeled AAA and AD , respectively. The heavy lines labeled T are two of the infinitely many branches of Efimov states. The cross-hatching indicates the threshold for scattering states.

In the discussion above, we have considered systems with identical mass which we will consider for the main part of this work. Nonetheless, it should be pointed out that the consequences of different masses on the discrete scale invariance/limit cycle are well-understood [2].

One-parameter correlations:

The necessity of two counterterms at leading order to obtain cutoff independent results implies that two very different types of one-parameter correlations exist. One can for example consider correlations between two- and three-body observables by changing the two-body counterterm and therefore effectively changing the scattering length. A well-known example of such a correlation is the so-called Efimov plot that is shown in Fig. 6. In this plot the binding momentum of the n th trimer state $K_n = \sqrt{mE_T^{(n)}}$ is plotted against the inverse scattering length. At the origin of the plot the three-body system shows the afore-mentioned exact discrete scaling symmetry with respect to the binding momenta along the y-axis. A change of L_3 in Eq. (24) corresponds therefore to a rescaling of the Efimov plot. Any point in this plot is therefore equally well-suited to characterize the short-distance behavior of the three-body amplitude and can be used instead of L_3 as the three-body parameter. Several distinct points are particularly convenient:

- κ_* , the binding momenta of a trimer in the limit $a \rightarrow \infty$,

- a'_* , the scattering length at which an Efimov trimer crosses the three-atom threshold,
- a_* , the scattering length at which an Efimov trimer crosses the dimer-atom threshold .

Other three-body parameters can of course be defined and generally all of them are related by simple expressions to each other, e.g. $a_* \approx 0.0798 \kappa_*^{-1}$ [2].

A very different type of correlation plot can be generated by keeping the two-body scattering length constant while varying the three-body force. This allows the study of the correlation between different three-body observables. One such correlation that is very well known is the Phillips line (which will be shown later). It is an approximately linear correlation between the particle-dimer scattering length and the three-body binding energy. This correlation line is well-known in nuclear physics, since calculations of the neutron-deuteron scattering length and triton binding energy with different two-nucleon potentials lie near this line.

Correlation lines calculated using the short-range EFT will in fact provide constraints on calculations with realistic potentials that give a large two-body scattering length. A three-body calculation of particle-dimer scattering length and binding energy employing such a potential has to give a point lying on or close to the Phillips line. The short-range EFT provides therefore strong low-energy constraints even in the absence of an experimental datum to fix the three-body low-energy constant.

Higher Orders and Higher Partial Waves:

The leading order (LO) calculations described above give results for the limit in which the range is taken to 0. The analysis of higher order corrections is important for several reasons. It allows to increase the accuracy of predictions for observables but provides also further information on the convergence radius of the short-range EFT. It was also mentioned before that the Lagrange density shown in Eq. (9) contains an infinite number of counterterms. It is therefore natural to ask at what order the next three-body force enters.

The calculation of higher order corrections has been addressed a number of times. The correction to observables linear in the effective range was already considered by Efimov using the hyperspherical formalism [24, 25] but no explicit results were given for systems in which the Efimov effect is relevant. Hammer and Mehen [26] calculated the next-to-leading order (NLO) correction to neutron-deuteron scattering perturbatively. They found an improvement in the description of the corresponding phase shift but didn't present a result for the three-body binding energy at NLO. The extension of their perturbative approach to higher orders is involved since it requires the knowledge of the full off-shell three-body scattering amplitude.

This and other publications displayed an unexpected convergence pattern since the NLO shift to LO observables was unexpectedly small. This lead to a more detailed analysis of the NLO correction to observables which is linear in the effective range [27]. It was found that the exact discrete scale invariance of the leading order wave function in the unitary limit protects the LO bound state

spectrum. That means, if $E_{T,\text{LO}}^{(n)}$ ($E_{T,\text{NLO}}^{(n)}$) denotes the binding energy of the n th three-body bound state at LO (NLO) in the limit $a \rightarrow \infty$, then we have

$$E_{T,\text{LO}}^{(n)} - E_{T,\text{NLO}}^{(n)} = 0 \quad \text{for all } n \text{ and } \gamma = 0. \quad (27)$$

This observation was made independently by Thøgersen, Fedorov and Jensen [28] using a numerical analysis of the Efimov bound state spectrum for finite range potentials.

For arbitrary scattering length, we can define the linear shift in the binding energy of the n th three-body bound state in the following way:

$$E_T^{(n)} = E_T^{(n^*)} \left[F_n \left(\frac{\gamma}{\kappa_*} \right) + \kappa_* r_s G_n \left(\frac{\gamma}{\kappa_*} \right) + \mathcal{O}[(\kappa r)^2] \right], \quad (28)$$

and we have $G_n(0) = 0$ for $\gamma = 0$. In Ref. [27] the function G_n was also analyzed for finite γ and evidence was found that G_n is close to 0 at the atom-dimer threshold. An ongoing analysis will shine more light on the properties of the linear range correction and will address the impact of finite range corrections on universal relations that relate the recombination maxima at negative scattering length to the recombination minima at positive scattering length and will give a better understanding of how different signatures of Efimov physics are impacted by finite range effects [29].

Bedaque *et al.* [30] calculated the neutron-deuteron phase shifts up to next-to-next-to-leading order (N²LO) and included (based on a perturbative power counting argument that assumes the cutoff to be $\Lambda \sim 1/R$) an additional energy-dependent three-body force at this order. They also suggested to include effective range corrections by modifying the two-body propagator in the STM equation. The two-body propagator with the effective range summed up to all orders is given by

$$D(p_0, \mathbf{p}) = \frac{1}{-\gamma + \frac{r_s}{2}(\gamma^2 + m p_0 - \mathbf{p}^2/4) + \sqrt{-m p_0 + \mathbf{p}^2/4}}. \quad (29)$$

It is easy to show that the denominator in Eq. (29) has two poles. In the case of positive γ and r_s this propagator has the bound state pole of the shallow dimer and a pole with binding energy

$$E_{\text{spurious}} = \frac{16}{m r_s^2} \left(1 - \frac{1}{2} \gamma r_s + \frac{1}{16} (r_s \gamma)^2 \right). \quad (30)$$

This pole corresponds to a spurious bound state which is unphysical since in the two-body system the short-range EFT cannot make predictions for energy scales $\gg 1/(mR^2)$. The spurious bound state pole in Eq. (29) leads to an ill-behaved kernel when inserted into the STM equation and the description of observables fails [31]. It was therefore suggested by Bedaque *et al.* to expand Eq. (29) in powers of the effective range:

$$\begin{aligned} D(p_0, \mathbf{p}) = & \frac{1}{-\gamma + \sqrt{-m p_0 + \mathbf{p}^2/4}} - \frac{r_s}{2} \frac{\gamma^2 + m p_0 - \mathbf{p}^2/4}{\left(-\gamma + \sqrt{-m p_0 + \mathbf{p}^2/4}\right)^2} \\ & + \left(\frac{r_s}{2}\right)^2 \frac{(\gamma^2 + m p_0 - \mathbf{p}^2/4)^2}{\left(-\gamma + \sqrt{-m p_0 + \mathbf{p}^2/4}\right)^3} + \dots \quad (31) \end{aligned}$$

This amounts to a partial resummation of effective range corrections when inserted into the STM equation. The difference in results for observables between a purely perturbative calculation of effective range corrections and this approach is expected to be of higher order. The solution of a modified STM integral equation leads directly to the desired observables and the amount of effort to calculate higher order corrections does therefore not increase compared to the solution of the leading order STM equation.

In Ref. [32] a renormalization group analysis was performed for large cutoffs in the STM equation. It lead to the conclusion that for large cutoffs no additional three-body counterterm has to be included until N3LO in the EFT expansion. Subsequent publications employing these results up N2LO found good agreement with experimental measurements and calculations using *realistic* interactions [33, 34].

There is an obvious disagreement between the predictions for the order at which the next three-body counterterm enters that requires a comment. In Ref. [30] it was argued that it enters at N2LO. In Ref. [32] the RG analysis lead to the conclusion that N3LO is the order at which an energy-dependent three-body force has to be included. The difference between the two analyses was the assumed size of the cutoff, namely either $\Lambda \sim 1/r_s$ or $\Lambda \gg 1/r_s$ which can in fact be the reason for the different conclusions. A future publication [29] will address this issue and will try to reconcile the results of Refs. [30] and [32].

An analysis of the power counting in higher partial waves was performed by Grißhammer [35]. He defined the asymptotic exponent s_l which describes the momentum behavior of the half off-shell amplitude for angular momentum l and for large off-shell momenta $p \gg k$

$$t_l(k, p) \propto k^l p^{-s_l-1} . \quad (32)$$

Using an argument based on the analysis of the perturbative evaluation of higher order corrections of the three-body amplitude, he identified the superficial degree of divergence of a given contribution at order n to be $n - 2s_l$. A contribution at order n will therefore diverge if

$$\text{Re}[n - 2s_l] \geq 0 . \quad (33)$$

Naively, one expects the large momentum behaviour of this amplitude to be determined by the driving term $K_l(k, p; E)$ of the STM equation

$$t_l(k, p) \propto \lim_{k \rightarrow 0} K_l(k, p, 3k^2/4) \propto k^l/p^{l+2} , \quad (34)$$

which would imply the simplistic estimate $s_l = l + 1$.

Grißhammer derived, however, an exact algebraic equation for the asymptotic exponent s_l using a Mellin transformation of the integral equation defined in Eq. (21) at zero energy

$$1 = (-1)^l \frac{2^{1-l}}{\sqrt{3\pi}} \frac{\Gamma\left[\frac{l+s+1}{2}\right] \Gamma\left[\frac{l-s+1}{2}\right]}{\Gamma\left[\frac{2l+3}{2}\right]} {}_2F_1\left[\frac{l+s+1}{2}, \frac{l-s+1}{2}; \frac{2l+3}{2}; \frac{1}{4}\right] . \quad (35)$$

system	$B^{(0)}$ [mK]	$B^{(1)}$ [mK]	$B_{\text{BG}}^{(0)}$ [mK]	$B_{\text{BG}}^{(1)}$ [mK]
${}^4\text{He}_3$	127	[2.186]	125.5	2.186
${}^4\text{He}_4$	492	128	559.7	132.7

Table 1. Binding energies of the ${}^4\text{He}$ trimer and tetramer in mK. The two right columns show the Monte Carlo results by Blume and Greene [45] (denoted by the index BG) while the two left columns show the EFT results of Platter, Hammer and Meißner [36]. The number in brackets was used as input to fix L_3 .

It depends only on the relative angular momentum l and the function ${}_2F_1[a, b; c; x]$ is the hyper-geometric series. The order n at which the first three-body force in particular partial wave channel enters can then be obtained from a solution of Eq. (35) and does for a number of cases not agree with the simplistic estimate derived from Eq. (34).

Equations (35) and (33) hold for spinless bosons. In Ref. [35] it was laid out how these formulas are generalized to systems of spin-1/2 nucleons.

2.4 The Four-Body System

It is natural to ask whether a new counterterm has to be included for every new particle added to the problem. The question whether a four-body parameter is required for consistent renormalization in the four-body system is therefore a logical extension of the effort of applying the short-range EFT to few-body systems. This pertinent question can also be paraphrased in more general terms: do zero-range two-body interactions and one three-body parameter lead to unique predictions for observables in the four-body sector?

This question was addressed in the framework of the short-range EFT by Platter, Hammer and Meißner in Ref. [36]. In this work the effective two- and three-body potentials at LO were generated and used together with the quantum mechanical few-body equations [37] to solve for the binding energies of the four-body system. The leading order effective two-body potential is given by

$$\langle \mathbf{k} | V | \mathbf{k}' \rangle = \lambda_2 g(k) g(k') , \quad (36)$$

here $g(k) = \exp(-k^2/\Lambda^2)$ is a regulator function. Since this is a separable potential, the two-body problem can be solved exactly [38]

$$t(E) = |g\rangle \tau(E) \langle g| , \quad (37)$$

with the two-body propagator τ

$$\tau(E) = [1/\lambda_2 - \langle g | G_0(E) | g \rangle]^{-1} , \quad (38)$$

and G_0 denotes the three-body propagator. Observables in the two-body sector will depend on the coupling strength λ_2 and the cutoff Λ . For a given cutoff Λ the coupling constant λ_2 is then renormalized by fixing the pole position of

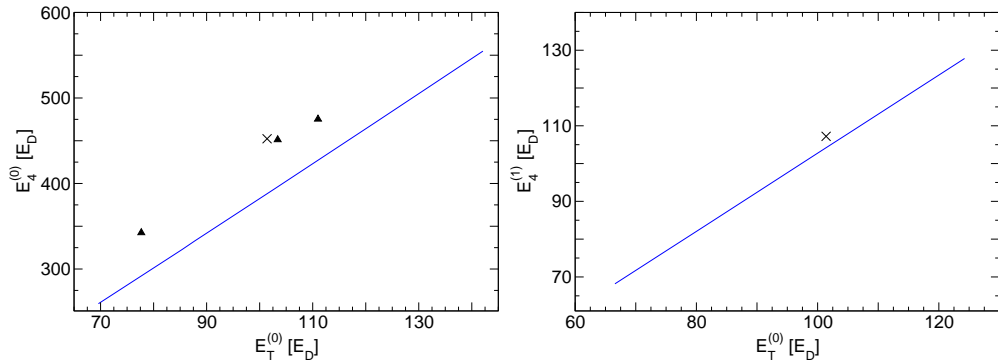


Figure 7. One-parameter correlations of three- and four-boson bound states. The crosses are results for LM2M2 potential [45]. The triangles are the results for the TTY, HFD-B and HFDHE2 potentials [46, 47].

the two-body propagator τ which amounts to fixing the binding energy of the two-body bound state. The effective three-body potential is

$$V_3 = \lambda_3 |\xi\rangle \langle \xi| , \quad (39)$$

where λ_3 denotes the three-body coupling constant that has to be adjusted to a three-body datum (such as the binding energy of the shallowest three-body bound state) and $\langle u_1 u_2 | \xi \rangle = \exp(-(u_1^2 - 3u_2^2/4)/\Lambda^2)$ is a regulator function (u_1 and u_2 denote here the canonical Jacobi momenta in the three-body system [37]).

Information on the necessity of a four-body parameter can be gained by studying the regulator dependence of four-body observables. A change in the regulator Λ corresponds to a modification of the short-distance physics while the renormalization conditions on the coupling constants λ_2 and λ_3 guarantee that low-energy observables in the two- and three-body sector remain unchanged. A detailed analysis shows then that no four-body parameter is required since the values of the tetramer binding energies converge to well-defined values with increasing regulator Λ [36].

This approach was also used to address the four-body problem of ${}^4\text{He}$ atoms. ${}^4\text{He}$ atoms have a scattering length 10 times larger than the range of the He-He interaction. The existence of n -body clusters of ${}^4\text{He}$ atoms was shown experimentally [40], however, the measurement of the binding energies of these cluster states is currently not possible. Several potentials that are believed to describe the two-body interaction accurately have been developed and have been used in Faddeev [41, 42, 43, 44] and Monte-Carlo [45] calculations. The four-body binding energies were computed, using the results for the dimer and trimer binding energies obtained using the LM2M2 potential in Ref. [45] as input. For the three-body coupling constant, the excited three-body state of the ${}^4\text{He}$ trimer was chosen as input parameter. The results can be seen in Table 1. The binding energies of the ${}^4\text{He}$ tetramer were found to be in good agreement with the results for the ground and excited state of the ${}^4\text{He}$ tetramer obtained by Blume and Greene [45].

By keeping the two-body parameter fixed and varying the three-body cou-

pling constant, the correlation line between the tetramer and trimer binding energies can be generated. These are approximately linear correlations which are well known from calculations in the few-nucleon sector. They parameterize the common knowledge that an internucleon potential that gives the correct value for the triton binding energy also gives a good result for the four-nucleon bound state (i.e. the α -particle). In Fig. 7 we show this correlation line (which in nuclear physics is called the Tjon line) generated for values of the three-body binding energy close to the value of ${}^4\text{He}$ trimer binding energy. The Tjon line is therefore a common feature of systems with a large two-body scattering length and does not depend on any details of the interaction at short-distances.

This approach was used furthermore for a more detailed analysis of the four-boson system with large positive and large negative scattering length [39]. Results in this analysis also lead to the conclusion that every trimer state is tied to two universal tetramer states with binding energies related to the binding energy of the next shallower trimer:

$$E_{4,0} \sim 5 E_T \quad \text{and} \quad E_{4,1} \sim 1.01 E_T \quad \text{for} \quad \gamma \sim 0, \quad (40)$$

where $E_{4,0}$ denotes the binding energy of the deeper of the two tetramer states and $E_{4,1}$ the shallower of the two.

A recent calculation by von Stecher, d’Incao and Greene [48] supports the findings made in [36, 39]. The authors of this work extended previous results to higher numerical accuracy. They furthermore considered the relation between universal three- and four-body bound states in the exact unitary limit ($a \rightarrow \infty$). They found

$$E_{4,0} \approx 4.57 E_T \quad \text{and} \quad E_{4,1} \approx 1.01 E_T, \quad (41)$$

which agree with the results obtained in Ref. [39] and given in Eq. (40).

The results obtained by the Hammer and Platter in Ref. [39] were furthermore presented in the form of an extended Efimov plot, shown in Fig. 8. Four-body states have to have a binding energy larger than the one of the deepest trimer state. The corresponding threshold is denoted by lower solid line in Fig. 8. The threshold for decay into the shallowest trimer state and an atom is indicated by the upper solid line. At positive scattering length, there are also scattering thresholds for scattering of two dimers and scattering of a dimer and two particles indicated by the dash-dotted and dashed lines, respectively. The vertical dotted line denotes infinite scattering length. A similar but extended version of this four-body Efimov plot was also presented by Stecher, d’Incao and Greene in Ref. [48]. They computed also the scattering lengths at which the binding energies of the tetramer states become zero and found

$$a_{4,0}^* \approx 0.43 a_* \quad \text{and} \quad a_{4,1}^* \approx 0.92 a_* . \quad (42)$$

A further interesting detail was pointed out in [48]. In the unitary limit the shallower of the two-four-body states can be considered as a trimer state with an extra particle attached to it. If this interpretation as an effective two-body state holds, then it leads to an important conclusion. Such an effective two-body picture in terms of a heavy and a light particle implies that the atom-trimer

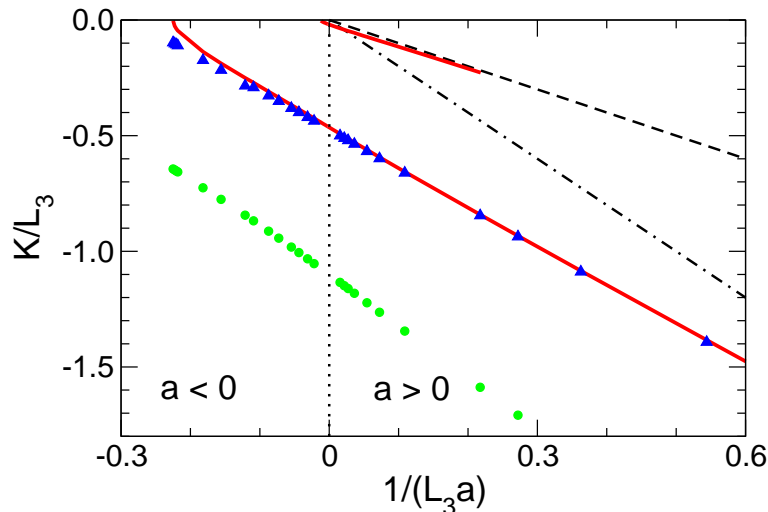


Figure 8. The a^{-1} - K plane for the four-body problem. The circles and triangles indicate the four-body ground and excited state energies $B_4^{(0)}$ and $B_4^{(1)}$, while the lower (upper) solid lines give the thresholds for decay into a ground state (excited state) trimer and a particle. The dash-dotted (dashed) lines give the thresholds for decay into two dimers (a dimer and two particles). The vertical dotted line indicates infinite scattering length. All quantities are given in units of the three-body parameter L_3 .

scattering length has to be large. For a two-body system with large positive scattering a length a and unequal masses, the binding energy is $1/(2\mu a^2)$, where $\mu = m_1 m_2 / (m_1 + m_2)$ is the reduced mass. With $m_1 = m$ and $m_2 = 3m$ we obtain for a_{AT}

$$E_T - E_{4,0} \approx \frac{2}{3} \frac{1}{m a_{AT}^2}, \quad (43)$$

where a_{aT} denotes the atom-trimer scattering length. We can therefore obtain a simple estimate for the scattering length of an Efimov trimer with index n and an atom in the unitary limit

$$a_{AT}^{(n)} = \sqrt{\frac{2}{3} \frac{1}{m(E_T - E_{4,0})}} \approx \sqrt{\frac{2/3}{0.01 m E_T^{(n)}}} \approx 8.2 \kappa_n^{-1}. \quad (44)$$

Since $E_T^{(n)}$ is the only scale in the problem, naive dimensional analysis predicts the range of the atom-trimer interaction to be of order κ_n^{-1} . The estimated scattering length a_{AT} is thus by an order of magnitude larger than this estimate of the range.

3 Low-Energy Universality in Atomic Physics

In this section we will discuss recent applications of the short-range EFT to systems of cold atoms. We will focus in particular on the problems of three-body recombination and atom-dimer relaxation in ultracold gases but will also report on recent progress in the four-body sector.

The recombination rate and atom-dimer relaxation have been identified as key signatures in the search for Efimov physics since they can be obtained by measuring atomic loss rates. Three-body recombination is a process in which a two-body bound state is formed as the result of a three-body collision. The two outgoing particles will gain kinetic energy in this process equal to the binding energy of the dimer. In experiments with ultracold atoms, the kinetic energy is often sufficient to allow the atom and dimer to subsequently escape the trapping potential.

Ultracold gases of alkali atoms are very well suited for such experiments since in many cases Feshbach resonances allow the scattering length to be tuned to arbitrarily large values using an external magnetic field. Observables can therefore be measured as a function of the two-body scattering length and results can be compared to the corresponding one-parameter correlation discussed previously.

The first experimental evidence for Efimov physics in an atomic system was presented by Grimm and co-workers [49]. In this pioneering experiment with ultracold ^{133}Cs atoms in the lowest hyperfine state, they observed a resonant enhancement in the 3-body recombination rate at $a \approx -850 a_0$ that can be explained with an Efimov trimer close to the 3-atom threshold.

Since then the number of experiments that show evidence for universal three-body physics has increased significantly. Signatures of Efimov physics have been found in three-component Fermi gases of ^6Li [50, 51], in a Bose gas of ^{39}K atoms [52], and in heterogeneous mixtures of ^{41}K and ^{87}Rb [53]. The level of sophistication in experiments has increased so much that recent measurements even test the implications of low-energy universality on four-body dynamics [54].

One experimental tool that has become essential for the analysis of Efimov physics are Feshbach resonances. As mentioned above they allow the interparticle scattering length to be tuned by adjusting an external magnetic field. A Feshbach resonance arises due to the coupling of two atoms in an open channel to a closed channel. The open channel corresponds to a pair of atoms in energetically allowed hyperfine states while the closed channel corresponds to a combination of hyperfine states that is energetically inaccessible to asymptotic scattering states. The coupling between the open and closed channel arises due to the hyperfine interaction. The scattering length becomes large when a magnetic field is used to tune a bound state in the closed channel to the threshold of the open channel. The dependence of the scattering length on the magnetic field near a Feshbach resonance can be described by

$$a(B) \approx a_{\text{bg}} \left(1 - \frac{\Delta}{B - B_0} \right), \quad (45)$$

where B_0 denotes the scattering at which a state in the closed channel is at threshold and Δ governs the width of the resonance. For magnetic fields away from the resonance B_0 , the scattering length is given by a_{bg} . The scattering length can therefore be tuned to values significantly larger than the low-energy length scale of the atom-atom interaction which is given by the so-called van der Waals length ℓ_{vdW} . This quantity is related to the long-range van der Waals tail

of the atom-atom interaction via

$$V(r) \rightarrow -\frac{\ell_{vdW}^4/m}{r^6} . \quad (46)$$

This length scale sets therefore the natural scale for the effective range $r_s \sim R$ of the interaction and quantifies at which distances the short-range EFT is not applicable anymore.

3.1 Three-Body Recombination of Identical Bosons

In a three-body recombination process, three particles collide and two of them form a two-body bound state. If the scattering length is large and positive, the resulting two-body bound state can be a *deep* dimer or a *shallow* dimer when the scattering length is positive. A deep dimer is a two-body bound state that cannot be described within the short-range EFT and has binding energy $\gtrsim 1/(mR^2)$. The shallow dimer can be described within the short-range EFT and has binding energy $\sim 1/(ma^2)$. If the scattering length is large and negative the resulting two-body bound state can only be a deep dimer.

The change in density n due to such losses is described by

$$\frac{d}{dt}n = -n_{\text{lost}}\alpha n , \quad (47)$$

where $n_{\text{lost}}\alpha \equiv L_3$ is an experimentally measurable loss rate constant, n_{lost} is the number of atoms escaping in every recombination process and α is the event rate of the recombination process. In the case of a Boltzmann distribution, the event rate can be related to the hyperangular averaged recombination rate $K(E)$:

$$\alpha(T) \approx \frac{\int_0^\infty dE E^2 e^{-E/(k_B T)} K(E)}{6 \int_0^\infty dE E^2 e^{-E/(k_B T)}} . \quad (48)$$

The recombination rate $K(E)$ can be decomposed into a contribution from recombination into the shallow dimer and a contribution from recombination into deep dimers:

$$K(E) = K_{\text{shallow}}(E) + K_{\text{deep}}(E) . \quad (49)$$

The three-body recombination rate into the shallow dimer can be decomposed into channel contributions with different total orbital angular momentum J :

$$K_{\text{shallow}}(E) = \sum_{J=0}^{\infty} K^{(J)}(E) . \quad (50)$$

The recombination rate K_{shallow} into the shallow dimer is then related to the total atom-dimer breakup cross section via

$$K_{\text{shallow}}(E) = \frac{192\sqrt{3}\pi(E_D + E)}{m^2 E^2} \sigma_{\text{breakup}}(E) . \quad (51)$$

This implies that the recombination rate is related to the S-matrix for the scattering of three atoms into an atom and dimer through the following relation:

$$K^{(J)}(E) = \frac{144\sqrt{3}\pi^2(2J+1)}{m^3 E^2} \sum_{n=3}^{\infty} \left| S_{AAA,AD}^{(J,n)}(E) \right|^2 . \quad (52)$$

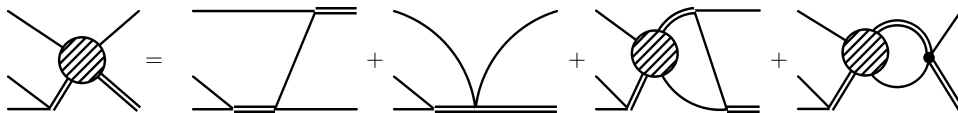


Figure 9. The integral equation for three-body recombination into the shallow dimer.

Here, n denotes a set of quantum numbers that includes the relative angular momenta between the particles. The hyperangular average is implemented by the sum over n which starts at $n = 3$ for convenience. The unitarity of the S-matrix in the angular momentum J sector implies

$$|S_{AD,AD}^{(J)}(E)|^2 + \sum_{n=3}^{\infty} |S_{AD,AAA}^{(J,n)}(E)|^2 = 1. \quad (53)$$

By unitarity, the recombination rate into the shallow dimer is therefore directly related to the S-matrix element for elastic atom-dimer scattering:

$$K^{(J)}(E) = \frac{144\sqrt{3}\pi^2(2J+1)}{m^3E^2} \left(1 - |e^{2i\delta_{AD}^{(J)}(E)}|^2 \right), \quad (54)$$

since

$$S_{AD,AD}^{(J)}(E) = e^{2i\delta_{AD}^{(J)}(E)}. \quad (55)$$

The phase shifts for atom-dimer scattering are therefore sufficient for a calculation of the recombination rate into shallow dimers.

Recombination into the Shallow Dimer:

Bedaque, Braaten and Hammer were the first to use the short-range EFT to describe three-body recombination into the shallow dimer [55]. They calculated the three-body recombination rate at zero temperature and for $J = 0$ by solving the integral equation for the scattering of three atoms into an atom and dimer, shown diagrammatically in Fig. 9. It can be shown that for zero energy, the amplitude for this process is related to the amplitude for elastic scattering given in Eq. (22) at an off-shell point. This can be used to simplify the numerical calculation of the three-body recombination rate. This approach can also be used to calculate the contribution to the recombination rate from channels with $J \neq 0$. The contribution to the three-body recombination rate is in this case

$$K^{(J)}(E) = \frac{144\sqrt{3}\pi^2(2J+1)f_J(x)}{x^4} \frac{a^4}{m}, \quad (56)$$

where $f_J(x)$ is a real-valued scaling function:

$$f_J(x) = 1 - \exp(-4 \operatorname{Im} \delta_{AD}^{(J)}(E)), \quad (57)$$

and x is defined as

$$x = (ma^2E)^{1/2}. \quad (58)$$

As $x \rightarrow 0$, the leading powers of x are determined by Wigner's threshold law [56]: $f_J(x) \sim x^{2\lambda_J+4}$, where $\lambda_1 = 3$ and $\lambda_J = J$ for $J \geq 2$.

It is only in the channel with total angular momentum $J = 0$ that observables depend on the three-body parameter. In this channel, a different perspective on the recombination rate can be gained using Efimov's radial [64, 2] laws which expresses the S-matrix in the three-body sector as a combination of universal functions of a scaling variable x and a phase θ_{*0} :

$$S_{AD,AD}^{(J=0)}(E) = s_{22}(x) + \frac{s_{21}(x)^2 e^{2i\theta_{*0}}}{1 - s_{11}(x)e^{2i\theta_{*0}}}, \quad (59a)$$

$$S_{AD,AAA}^{(J=0,n)}(E) = s_{2n}(x) + \frac{s_{21}(x)s_{1n}(x)e^{2i\theta_{*0}}}{1 - s_{11}(x)e^{2i\theta_{*0}}}. \quad (59b)$$

The phase θ_{*0} is related to the minimum in the recombination rate a_{*0} for positive scattering length

$$\theta_{*0} = s_0 \ln(a/a_{*0}), \quad (60)$$

where $a_{*0} \approx 0.32\kappa_*^{-1}$ [2].

Using analytical results on the atom-dimer phase shift at breakup threshold obtained in Ref. [57], Efimov's radial laws can be used to derive an analytical result for the recombination rate into the shallow dimer

$$K^{(0)}(E=0) = \frac{768\pi^2(4\pi - 3\sqrt{3}) \sin^2[s_0 \ln(a/a_{*0})] a^4}{\sinh^2(\pi s_0) + \cos^2[s_0 \ln(a/a_{*0})] m}. \quad (61)$$

Macek, Ovchinnikov and Gasaneo derived this analytic result for the three-body recombination rate at the three-atom threshold in [58]. This equation was also derived independently by Petrov [59]. Simpler approximate expressions that correspond essentially to omitting the \cos^2 term in the denominator have been previously derived by Nielsen and Macek [60], Esry, Green and Burke [61] and by Bedaque, Braaten and Hammer [55].

For a fixed scattering length, the recombination rate in Eq. (61) has therefore the maximum value

$$K_{\max} = 6C_{\max}a^4/m \quad \text{with} \quad C_{\max} = \frac{128\pi^2(4\pi - 3\sqrt{3})}{\sinh^2(\pi s_0)}. \quad (62)$$

Effects of Deep Dimers:

While recombination into the shallow dimer can only occur for positive scattering length, recombination into deeply bound states (into deep dimers) can occur for either sign of the scattering length. Properties of these bound states cannot be calculated in the short-range EFT. However, their cumulative effects on low-energy observables can be accounted for analytically continuing the Efimov parameter to complex values. This introduces only one additional real-valued parameter denoted usually with η_* . If the dependence of an amplitude on κ_* or, equivalently, a_{*0} is known analytically, the effect of deep dimers can be taken into account by the simple substitution

$$\ln a_{*0} \longrightarrow \ln a_{*0} - i\eta_*/s_0 \quad (63)$$

For positive scattering length, making this replacement in the amplitudes for recombination into the shallow dimer leads to

$$K_{\text{shallow}}(0) = \frac{768\pi^2(4\pi - 3\sqrt{3})(\sin^2[s_0 \ln(a/a_{*0})] + \sinh^2 \eta_*)}{\sinh^2(\pi s_0 + \eta_*) + \cos^2[s_0 \ln(a/a_{*0})]} \frac{a^4}{m}, \quad (64)$$

Using unitarity, one can also obtain an analytic expression for the recombination rate into deep dimers:

$$K_{\text{deep}}(0) = \frac{384\pi^2(4\pi - 3\sqrt{3}) \coth(\pi s_0) \sinh(2\eta_*)}{\sinh^2(\pi s_0 + \eta_*) + \cos^2[s_0 \ln(a/a_{*0})]} \frac{a^4}{m}, \quad (a > 0). \quad (65)$$

These results were first derived by Braaten and Hammer [2]. Simpler approximate expressions that correspond essentially to omitting the \cos^2 in the denominator were derived in Ref. [62]. The weak dependence on the three-body parameter a_{*0} in Eq. (65) was first observed in a numerical calculation for the case of infinitesimal η_* [63].

For negative scattering length, there is no shallow dimer. The recombination rate into deep dimers is given by

$$K_{\text{deep}}(0) = \frac{765 \sinh(2\eta_*)}{\sin^2(s_0 \ln(a/a'_*)) + \sin^2 \eta_*} \frac{a^4}{m}, \quad (a < 0). \quad (66)$$

This results was first derived by Braaten and Hammer in Ref. [62]. The scaling of K_{deep} with a^4 was predicted by Nielsen and Maceck and by Esry *et al.* [60, 61]. Esry *et al.* were the first to point out the existence of a log-periodic sequence of resonances related to Efimov trimers [61].

Three-Body Recombination at Finite Temperature:

The experimental measurements of the three-body recombination rate of ^{133}Cs atoms were performed at finite temperature. Although the zero temperature equations can be applied immediately to their results, it is desirable to extend these to finite temperature. This requires the calculation of the energy dependent recombination rate. For recombination into the shallow dimer, this can be obtained by solving the amplitude for scattering of three atoms into atom and dimer as a function of the external momenta, calculating the thermal average of the recombination rate, and then adjusting the three-body parameters κ_* and η_* to fit experimental data. An alternative path is to determine the universal functions $s_{ij}(x)$ from the atom-dimer scattering phase shifts. Once these functions are determined, the temperature dependent recombination rate can be determined for any system of identical bosons with arbitrary three-body parameter. This was done in Ref. [65] for the case of positive scattering length. Using the STM equation the atom-dimer phase shifts were calculated for a wide range of energies and three-body parameters. The results were then fit to the formula

$$\exp\left(2i\delta_{AD}^{(J=0)}(E)\right) = s_{22}(x) + \frac{s_{12}(x)^2 \exp[2is_0 \ln(a/a_{*0})]}{1 - s_{11}(x) \exp[2is_0 \ln(a/a_{*0})]} \quad (67)$$

to determine the universal scaling functions $s_{11}(x)$, $s_{12}(x)$ and $s_{22}(x)$ for $0 < x < 10$.

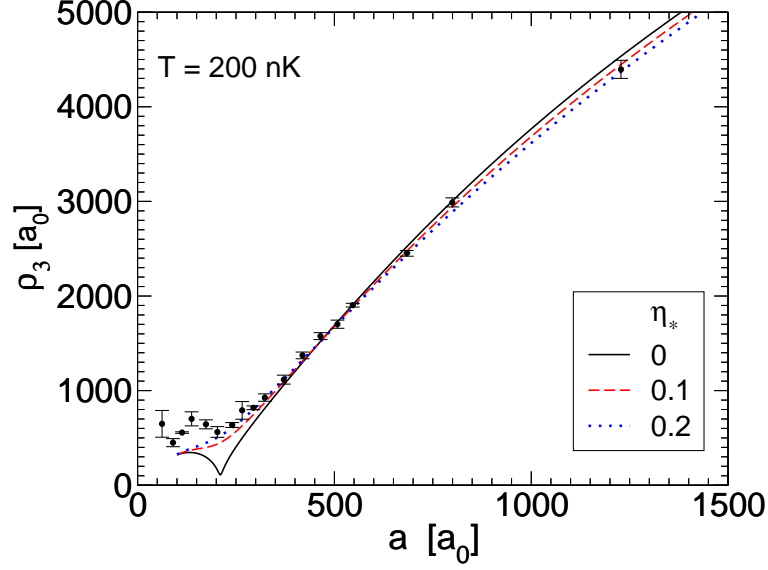


Figure 10. The 3-body recombination length ρ_3 for ^{133}Cs atoms as a function of a for $T = 200$ nK. The data points are from Ref. [49]. The curves are the universal prediction for three values of η_* : 0 (solid line), 0.1 (dashed line), and 0.2 (dotted line).

Using the unitarity of the S-matrix it can then be shown that these three universal scaling functions are sufficient for the calculation of the $J = 0$ contributions to the recombination rate into shallow dimers, even if there are deep dimers:

$$K^{(0)}(E) = \frac{144\sqrt{3}\pi^2}{x^4} \left(1 - \left| s_{22}(x) + \frac{s_{12}(x)^2 e^{2i\theta_{*0} - 2\eta_*}}{1 - s_{11}(x) e^{2i\theta_{*0} - 2\eta_*}} \right|^2 \right) \quad (68)$$

$$- \frac{(1 - e^{-4\eta_*}) |s_{12}(x)|^2}{|1 - s_{11}(x) e^{2i\theta_{*0} - 2\eta_*}|^2} \frac{a^4}{m}, \quad (69)$$

They are also sufficient to calculate the recombination rate into deep dimers:

$$K_{\text{deep}}(E) = \frac{144\sqrt{3}\pi^2 (1 - e^{-4\eta_*}) (1 - |s_{11}(x)|^2 - |s_{12}(x)|^2)}{x^4 |1 - s_{11}(x) e^{2i\theta_{*0} - 2\eta_*}|^2} \frac{a^4}{m}. \quad (70)$$

The knowledge of three universal scaling functions facilitates therefore the calculation of the temperature dependent recombination rate constant in the presence of deep dimers. In Fig. 10 the theoretical results for three different values of η_* are compared to the experimental results by Grimm and co-workers. The vertical axis is the recombination length ρ_3 defined by

$$\rho_3 = \left(\frac{2m}{\sqrt{3}} n_{\text{lost}} \alpha \right)^{1/4}, \quad (71)$$

where n_{lost} .

The recombination minimum that determines the three-body body input is near $200 a_0$. This is comparable in size to the Waals length scale $(mC_6)^{1/4} \approx$

$200 a_0$, so range corrections may be large near the minimum and the disagreement between theoretical and experimental results at smaller values of the scattering length is hardly surprising. The authors of Ref. [65] were not able to determine η_* since their fit was insensitive to the value of η_* . It yielded, however, the upper bound $\eta_* < 0.2$. Their result for the recombination minimum $a_{\min} = 210(10) a_0$ obtained from a fit for $a > 500 a_0$ agrees with direct experimental loss measurements performed by the Innsbruck group.

Finite Range Effects in Three-Body Recombination:

The recombination rate measurements performed by Grimm and co-workers were carried out at scattering lengths at which the finite range of the atom-atom interaction is expected to play a significant role. The range of the ^{133}Cs interaction is of the order of $200 a_0$. It is therefore of interest to understand the impact of the finite range of the atom-atom interaction on experimentally measurable quantities.

A first effort to calculate range corrections to the recombination rate into shallow dimers was performed in [66]. The authors considered corrections up to N2LO in the EFT expansion to the recombination rate and calculated the correlation between the atom-dimer scattering length and the recombination rate $K(0)$ at zero energy. The approach was furthermore used to calculate the recombination rate coefficient for ^4He atoms for which the effective range is known. This approach can be applied to more interesting systems such as ^{133}Cs or ^6Li provided the corresponding effective range is known.

3.2 Three-Body Recombination of Fermions

A large number of experiments with cold atoms are now carried out with fermionic atoms. Systems of fermionic atoms are of interest due to their relation to solid state physics. In particular, systems with two spin states have received considerable attention. Many-body systems of cold atoms display superfluidity at sufficiently low temperatures. Feshbach resonances can be used to study how the mechanism for superfluidity depends on the interactions. In the case of fermions with two spin states, as the scattering length is varied from $1/a < 0$ to $1/a > 0$ through the Feshbach resonance, the mechanism changes continuously from the formation of Cooper pairs to the Bose-Einstein condensation of shallow dimers.

The Efimov can not occur in systems of fermions with only two spin states. This can be understood from the fact that a pointlike three-body S -wave interaction is forbidden due to the Pauli principle. However, in the case of fermions with three spin states the Efimov effect can occur again since a pointlike three-body S -wave interaction is not forbidden by the Pauli principle. Experiments using ^6Li atoms in the three lowest hyperfine states have been performed by Selim and co-workers [50] and O'Hara and co-workers [51]. The three corresponding scattering lengths in this system have broad Feshbach resonances at nearby values of the magnetic field, i.e. at 690 G, 810 G and 833 G. A narrow loss feature near 130 G was discovered independently by both groups. At these magnetic field strengths all three scattering lengths are negative and relatively large, universal results are therefore relevant in this region and the short-range EFT is applicable.

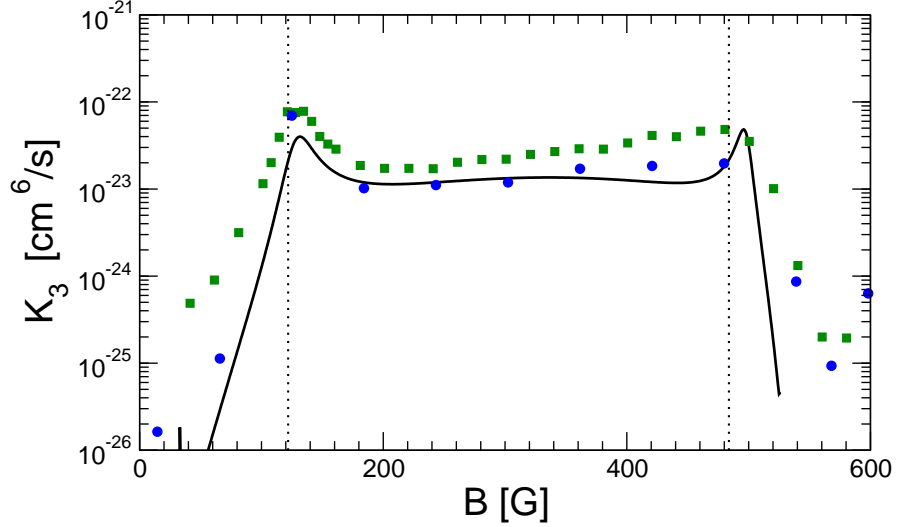


Figure 11. The 3-body recombination rate constant K_3 for the three lowest hyperfine spin states of ${}^6\text{Li}$ atoms as a function of the magnetic field B . The two vertical dotted lines mark the boundaries of the region in which $|a_{12}| > 2 \ell_{\text{vdW}}$. The solid squares are data points from Ref. [50]. The solid dots are data points from Ref. [51]. The curve is a 2-parameter fit to the shape of the data from Ref. [50].

The rate equations for the number densities n_i of atoms in the three spin states are

$$\frac{d}{dt}n_i = -K_3 n_1 n_2 n_3. \quad (72)$$

In the case of this more complicated system, no analytical results for the recombination rate are available so one has to do a numerical calculation. The three-body recombination is related to the amplitudes for elastic scattering

$$K_3 = \frac{32\pi^2}{m} \sum_{i,j} a_i a_j \text{Im} A_{ij}(0,0), \quad (73)$$

The amplitudes A_{ij} have to be calculated from a set of nine coupled integral equations which are an extension of the STM equation:

$$A_{ij}(p,0) = \frac{1 - \delta_{ij}}{p^2} + \frac{2}{\pi} \sum_k (1 - \delta_{kj}) \int_0^A dq \frac{q}{2p} \ln \left(\frac{p^2 + pq + q^2}{p^2 + pq + q^2} \right) \times \frac{A(q,0)}{-1/a_k + \sqrt{3}/2q}. \quad (74)$$

These equations are written out without the use of an explicit three-body force and instead the momentum cutoff is used to fix the the three-body coefficient. In [67] the recombination rate of general systems of three identical fermions with three spin states was analyzed. The case of ${}^6\text{Li}$ was also considered. Theoretical results on the magnetic field dependence of the three scattering lengths were used to calculate the three-body recombination rate in regions of the magnetic

field relevant to the Penn-State and Heidelberg experiments. The effects of deep dimers were included by using a complex cutoff $\Lambda e^{i\eta_*/s_0}$ in the STM integral equation in Eq. (74). The three-body parameters were adjusted to reproduce the observed recombination maximum near 130 G. In Fig. 11 we show a comparison of theoretical and experimental results. The results are in excellent agreement with the observed recombination rate near the narrow loss feature at 210 G. They also predict a second narrow loss feature near 500 G. In the experiments a broad loss feature is observed near 500 G, but the behavior in this region is not correctly reproduced by theory. The reason for this discrepancy is under investigation.

Following this work, the problem was also considered using a wave function approach [68] and functional renormalization [69]. The authors of both studies found qualitative agreement with the EFT results.

3.3 Atom-Dimer Relaxation

Another observable closely related to three-body recombination is atom-dimer relaxation. If there is an Efimov trimer close to the three-atom threshold, inelastic scattering processes of atom-dimer to atom-(deep dimer) will be resonantly enhanced. The parameters that determine the rate of these losses are a , κ_* and η_* .

The relaxation rate event constant is defined by the following equation:

$$\frac{d}{dt}n_A = \frac{d}{dt}n_D = -\beta n_A n_D, \quad (75)$$

where n_A denotes the atom density and n_D denotes the density of dimers. The rate constant β can also be obtained using the optical theorem:

$$\beta = -\frac{6\pi}{m} \text{Im} a_{AD}, \quad (76)$$

where a_{AD} denotes the atom-dimer scattering length:

$$\beta = \frac{20.3 \sinh(2\eta_*)}{\sin^2(s_0 \ln(a/a_*)) + \sinh^2 \eta_*} \frac{a}{m}, \quad (77)$$

where a_* denotes the value of the two-body scattering length at which there is a trimer at the atom-dimer threshold: $a_* \approx 0.0798 \kappa_*^{-1}$. This expression was first derived in [62] using Efimov's radial law discussed in the previous section.

Atom-dimer relaxation at finite temperature was first considered by Braaten and Hammer in Ref. [70]. Recently, Helfrich and Hammer [71] extended this work. Using generalized Bose-Einstein distribution functions to perform a thermal average, they calculated the rate of change in the number of shallow dimers N_D due to relaxation into deep dimers:

$$\frac{d}{dt}N_D = - \int d^3r d^3p_A d^3p_D n_A(p_A, r) n_D(p_D, r) \frac{3k}{2m} \sigma_{AD}^{\text{inel}}, \quad (78)$$

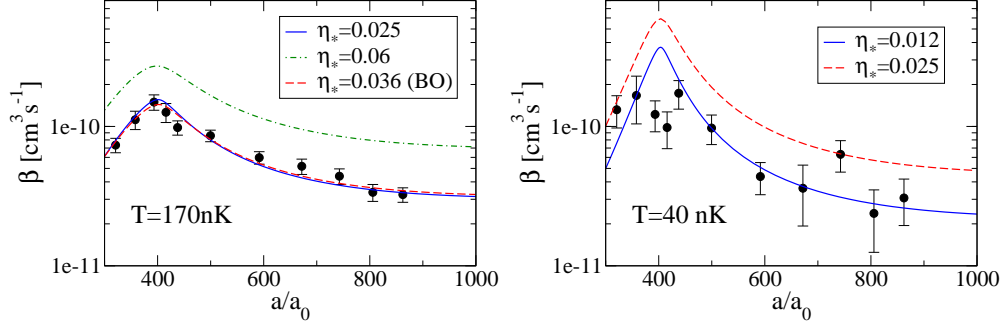


Figure 12. Left: The dimer relaxation coefficient β as a function of a/a_0 for $T = 170$ nK, $a_* = 395a_0$, and different values of η_* . BO indicates a Boltzmann average. Right: β as a function of a/a_0 for $T = 40$ nK, $a_* = 395a_0$, and different values of η_* . The data points in both panels are from [72].

here $k = |2\mathbf{p}_A - \mathbf{p}_D|/3$ denotes the relative momentum, \mathbf{p}_A and \mathbf{p}_D are the momenta of atoms and dimer, respectively. The generalized Bose-Einstein distribution functions $n_{A/D}$ for atoms/dimers in a harmonic trapping potential are

$$n_i(p_i, r) = \left\{ \exp \left[\left(\frac{p_i^2}{2m_i} + \frac{m_i \omega^2 r^2}{2} - \mu_i \right) / (k_B T) \right] - 1 \right\}^{-1}, \quad (79)$$

with $i = A, D$, ω denotes the average trap frequency, and μ_i is the chemical potential. Knowledge of the S -wave phase shift for atom-dimer scattering δ_0^{AD} allows therefore the evaluation of Eq. (78) since $\sigma_{AD}^{\text{inel.}} = \sigma_{AD}^{\text{total}} - \sigma_{AD}^{\text{elastic}}$ and

$$\begin{aligned} \frac{d\sigma_{AD}^{\text{elastic}}}{d\Omega} &= \left| \frac{1}{k \cot \delta_0^{AD} - ik} \right|^2, \\ \sigma_{AD}^{\text{total}} &= \frac{4\pi}{k} \text{Im} \left(\frac{1}{k \cot \delta_0^{AD} - ik} \right), \end{aligned} \quad (80a)$$

Braaten and Hammer have calculated the phase shift $ka \cot \delta_0^{AD}$ for k up to the dimer breakup threshold $\sqrt{3}/(2a)$ [62]. They parameterized the results as

$$ka \cot \delta_0^{AD}(k) = c_1(ka) + c_2(ka) \cot [s_0 \ln(0.19 a/a_*) + \phi(ka)], \quad (81)$$

where

$$\begin{aligned} c_1(ka) &= -0.22 + 0.39k^2 a^2 - 0.17k^4 a^4, \\ c_2(ka) &= 0.32 + 0.82k^2 a^2 - 0.14k^4 a^4, \\ \phi(ka) &= 2.64 - 0.83k^2 a^2 + 0.23k^4 a^4. \end{aligned} \quad (82)$$

Using these results Helfrich and Hammer evaluated the integral in Eq. (78). They related their results to the experimental results by Knoop *et al.* [72] using the loss model employed in [72]. They find

$$\beta \equiv -\frac{\sqrt{27}}{8\bar{n}_A N_D} \frac{d}{dt} N_D. \quad (83)$$

The factor of $(\sqrt{3}/2)^3$ takes into account the assumed Boltzmann distributions $\exp(-m_i\omega^2 r^2/3)$ of the atoms and the dimers that were assumed in the analysis of Ref. [72].

The free parameters a_* and η_* are fitted to the data at $T = 170$ nK. In the left panel of Fig. 12, the results for $a_* = 395a_0$ and $\eta_* = 0.025, 0.06$ (solid curves) give an excellent fit to the experimental results by Knoop *et al.* [72]. The dashed curve in the left panel is the result one obtains by using a Boltzmann instead of a Bose-Einstein distribution in Eq. (79). The results display some sensitivity to η_* . At $T = 40$ nK, the best fit is obtained with $\eta_* = 0.012$ (solid line). The value $\eta_* = 0.025$, which gave the best fit for 170 nK gives a prediction that is too large by a factor of two when compared to the experimental results.

3.4 Four-Body Recombination

Stecher, d’Incao and Greene considered in their work on the four-body system also the implications of 4-body universality on loss rates in systems of ultracold atoms [73]. In particular, they pointed out that the existence of the two universal tetramer states discovered by Platter and Hammer should lead to observable loss features at values of the scattering length that are related to the scattering length at which the tetramer binding energy becomes zero. Their results for the values of the scattering lengths are given in Eq. (42).

In a second paper Stecher, d’Incao and Greene addressed the problem of dimer-dimer collisions [73] which is relevant for the case of positive scattering length. They denoted the two-body scattering length for which the i th four-body bound state crosses the dimer-dimer threshold by $a_{dd,i}^*$. They denoted the two-body scattering length at which the trimer-atom and dimer-dimer channels become degenerate by a_{dd}^c . We previously defined a_* to be the scattering length at which the trimer state crosses atom-dimer threshold. The ratio of these quantities are universal numbers

$$a_{dd,0}^*/a_{dd}^c \approx 2.37, \quad a_{dd,1}^*/a_{dd}^c \sim 6.6, \quad \text{and} \quad a_{dd}^c/a_* \approx 6.73. \quad (84)$$

Ferlaino *et al.* recently studied the four-body problem with short-range interactions experimentally [54]. Using ultracold ^{133}Cs atoms in the lowest hyperfine state at a temperature of 50 nK, they found loss features at scattering lengths $-730a_0$ and $-410a_0$ which were interpreted as the four-body loss features predicted by Stecher, d’Incao and Greene [48]. With the triatomic Efimov resonance measured at $-870a_0$, this gives for the ratios of the four- and three-body resonance position

$$a_{4,0}^*/a_* \approx 0.47 \quad \text{and} \quad a_{4,1}^*/a_* \approx 0.84. \quad (85)$$

These experimental results are in fact surprisingly close to the zero-range prediction made in [48] since finite range effects are expected to be important at these values of the scattering length. The range of the Cs-Cs interaction (which is set by the van-der Waals length scale) is approximately $200a_0$.

3.5 Challenges and Opportunities I

Recent experimental progress demonstrates that the limits of complexity have not been reached yet in the field of few-body dynamics in gases of ultracold atoms. The experimental evidence for three-body universality in systems of ultracold atoms has increased significantly. First experimental evidence for four-body universality have been presented and more can be expected in the near future.

Measurements of Efimov loss features in heterogeneous systems, i.e. systems with different constituent masses, have also been presented. It is therefore a natural task to identify the universal signatures and their relation to each other using the short-range EFT. Some of these signatures might offer also stronger signatures of Efimov physics since the discrete scaling factor associated with the Efimov bound state spectrum depends on the mass ratios of the constituents.

Significant progress in mapping out the relevant signatures of universal four-body physics has been made. However, a full treatment of scattering processes remains desirable. This would facilitate an analysis of the impact of universality on further quantities such as the dimer-dimer or atom-trimer scattering lengths. Access to scattering quantities is also required for the calculation of the four-body recombination rate at finite temperature.

The ongoing analysis of the effects of range corrections on universal few-body physics is important since most experiments are carried out at scattering lengths at which the finite range of the two-body interaction is expected to have a measurable effect. The questions that remain to be answered are therefore how universal relations that relate different recombination observables will be affected by finite range effects and what implications does a small but finite range have for the four-body bound state spectrum. Since the linear range correction has been shown to be small for some observables it will be important to address the quadratic range correction with a full N²LO analysis.

4 Low-Energy Universality in Nuclear Physics

The model-independent description of nuclear systems has been one of the main goals in nuclear physics for many years. Since their introduction to nuclear physics, EFTs have allowed the calculation of a large number of observables model-independently and in some cases to very high accuracy. The *standard* EFT approaches to internucleon interactions employ nucleon and pion fields as the minimal set of degrees of freedom [74, 4, 5]. The separation of scales that is exploited here is the one of chiral symmetry which identifies pions as the Goldstone bosons of the spontaneously broken chiral symmetry of QCD. The relatively small pion mass is then a consequence of the small up and down quark mass, i.e. the explicitly broken chiral symmetry.

Fortunately, this is not the only separation of scales in the two-nucleon system. It turns out that also the scattering length in the nucleon-nucleon system is large compared to the range of the interaction which in this case is set by the pion mass m_π . The short-range EFT can therefore be applied in the nuclear sector as long as we consider momenta that are much smaller than m_π .

Such a limitation might seem to make this approach inadequate for nuclear

physics. However, it is important to realize that a large number of reactions relevant to nuclear astrophysics occur at energies well below this breakdown scale of the *short-range* EFT. Proton-proton fusion ($p+p \rightarrow {}^2\text{H}+e^++\nu_e$) for example, a reaction which plays an important role in the sun's energy generation, occurs at the keV scale due to the *low* temperature in the sun. The short-range EFT seems therefore to be the ideal framework for the calculation of such reaction.

Halo nuclei and weakly bound systems of α particles are an additional playground for the short-range EFT. Halo nuclei are weakly bound systems of a core (e.g. an α -particle) and additional nucleons that are weakly bound to the core. There is also evidence that some of the properties of α -clusters can be described using the short-range EFT.

In this section we will discuss applications of the short-range EFT to systems of nucleons. We will first consider the two-nucleon system and discuss a recent calculation in this sector which exemplifies the strong predictive power of the short-range EFT. We will then turn to the three-nucleon sector. We will discuss the renormalization, the inclusion of higher order corrections and the status of the inclusion of external currents in the few-body sector. Then we summarize recent calculation of halo nuclei. We end with a subsection which discusses the work required to be done in the future.

4.1 Two Nucleons

Nucleons are spin 1/2 particles that come in two flavors, protons and neutrons. A nucleon field will therefore carry spin and isospin indices to accommodate these extra degrees of freedom. The Lagrange density for nucleons interacting at very low energies is constructed by writing down all possible operators allowed by the underlying symmetries

$$\begin{aligned} \mathcal{L} = & N^\dagger \left(i\partial_0 + \frac{\nabla^2}{2m} \right) N - C_0^t (N^T \tau_2 \sigma_i \sigma_2 N)^\dagger (N^T \tau_2 \sigma_i \sigma_2 N) \\ & - C_0^s (N^T \sigma_2 \tau_a \tau_2 N)^\dagger (N^T \sigma_2 \tau_a \tau_2 N) + \dots, \quad (86) \end{aligned}$$

where the dots represent higher-order contributions suppressed by more fields and/or derivatives. The low-energy constants C_0^s and C_0^t are renormalized to the spin-singlet and triplet scattering length, respectively.

The short-range EFT has been applied very successfully in the two-nucleon sector to electroweak observables. Here, we will only mention a few very recent calculations since they exemplify typical applications and the predictive power for low-energy processes with only a few physical input parameters.

Christlmeier and Griebhammer [75] recently addressed a discrepancy between previously obtained theoretical and experimental results for the electrodisintegration cross section of deuterium (${}^2\text{H}(e, e'p)n$). They considered the triple-differential cross-section for this process which can also be decomposed into

$$\begin{aligned} \frac{d^3\sigma}{dE_e^{\text{lab}} d\Omega_e^{\text{lab}} d\Omega_p} = & \frac{d^3}{dE_e^{\text{lab}} d\Omega_e^{\text{lab}} d\Omega_p} (\sigma_L + \sigma_T \\ & + \sigma_{LT} \cos \Phi_p + \sigma_{TT} \cos 2\Phi_p) \quad , \quad (87) \end{aligned}$$

where $\Omega_e^{\text{lab}} = (\Theta_e^{\text{lab}}, \Phi_e^{\text{lab}} \equiv 0)$ and $\Omega_p = (\Theta_p, \Phi_p)$ are the scattering angles of electron and proton in the lab frame, respectively. The superscript ‘‘lab’’ denotes the laboratory frame which is defined to be the rest frame of the deuteron. They found their results to be in excellent agreement with previous theoretical calculations by Arenh ovel *et al.* [76] and Tamae [77] which lead to the conclusion that none of the available theoretical approaches can explain the experimental data presented for σ_{LT} in Ref. [78]. A subsequent experimental study of the double differential cross section for $({}^2\text{H}(e, e'p)n)$ at an angle of 180° lead to excellent agreement between experiment and theory [79].

Finally, Ando considered $pp \rightarrow pp\pi^0$ near production threshold in the short-range EFT [80] and Phillips, Schindler and Springer considered parity violating nucleon-nucleon scattering in [81].

4.2 Three Nucleons

The short-range EFT was first applied to three-nucleon systems by Bedaque, Hammer and van Kolck [82, 83]. As in the bosonic case, the calculation of three-body processes is simplified if we introduce auxiliary fields that carry the quantum numbers of the allowed two-body S -wave states. Here, we introduce two auxiliary fields (one for every possible S -wave channel), t_i with spin 1 (isospin 0) and s_i with spin 0 (isospin 1), respectively

$$\begin{aligned} \mathcal{L} = & N^\dagger(i\partial_0 + \frac{\nabla^2}{2M})N - t_i^\dagger(i\partial_0 + \frac{\nabla^2}{4M} - \Delta_t)t_i - s_j^\dagger(i\partial_0 + \frac{\nabla^2}{4M} - \Delta_s)s_j \\ & + g_t \left(t_i^\dagger N^T \tau_2 \sigma_i \sigma_2 N + \text{h.c.} \right) + g_s \left(s_j^\dagger N^T \sigma_2 \sigma_j \tau_2 N + \text{h.c.} \right) \\ & - G_3 N^\dagger \left(g_t^2 (t_i \sigma_i)^\dagger t_{i'} \sigma_{i'} + \frac{1}{3} g_t g_s [(t_i \sigma_i)^\dagger s_j \tau_j + \text{h.c.}] \right. \\ & \left. + g_s^2 (s_j \tau_j)^\dagger s_{j'} \tau_{j'} \right) N + \dots, \quad (88) \end{aligned}$$

We want to use this Lagrange density to calculate observables for nucleon deuteron scattering. The total spin of this system is either 1/2 (singlet) or 3/2 (quartet) and correspondingly two different integral equations can be derived that describe the scattering of a neutron and a deuteron in a relative S -wave. The integral equation for scattering in the quartet channel is given by

$$t_{3/2}(p, k) = -\frac{4\pi\gamma_t}{m} K(p, k) - \frac{1}{\pi} \int_0^\infty dq q^2 D_s(q) K(p, q) t_{3/2}(q, k), \quad (89)$$

where

$$K(p, k) = \frac{1}{pk} \ln \left(\frac{p^2 + pk + k^2}{p^2 - pk + k^2} \right). \quad (90)$$

The Pauli principle forbids the appearance of an S -wave three-body force in this channel, since the spins and isospins of two of the three nucleons are aligned parallelly.

The integral for the scattering in the singlet channel is given by

$$\begin{aligned}
t_{1/2}^s(p, k) &= \frac{8\pi\gamma_t}{m} \left(\frac{3}{4}K(p, k) + \frac{2H}{\Lambda^2} \right) + \frac{1}{2\pi} \int_0^\Lambda dq^2 D_s(q) \left(K(q, p) + \frac{2H}{\Lambda^2} \right) t_s(q, k) \\
&\quad + \frac{1}{2\pi} \int_0^\Lambda dq^2 D_t(q) \left(K(q, p) + \frac{2H}{\Lambda^2} \right) t_s(q, k) \\
t_{1/2}^t(p, k) &= \frac{8\pi\gamma_t}{m} \left(\frac{1}{4}K(p, k) + \frac{2H}{\Lambda^2} \right) + \frac{1}{2\pi} \int_0^\Lambda dq^2 D_t(q) \left(K(p, q) + \frac{2H}{\Lambda^2} \right) t_s(q, k) \\
&\quad + \frac{1}{2\pi} \int_0^\Lambda dq^2 D_s(q) \left(K(p, q) + \frac{2H}{\Lambda^2} \right) t_s(q, k) .
\end{aligned} \tag{91}$$

In this case a three-body force is allowed and also required for consistent renormalization of the problem. The triton binding energy can be calculated from the homogeneous part of Eq. (91) since the total spin (isospin) of the triton is $1/2$ ($1/2$).

The solutions of Eqs. (89) and (91) are related to the deuteron-neutron phase shift

$$t_{3/2}(k, k) = \frac{3\pi}{m} \frac{1}{k \cot \delta_{3/2} - ik} , \tag{92a}$$

$$t_{1/2}^t(k, k) = \frac{3\pi}{m} \frac{1}{k \cot \delta_{1/2} - ik} . \tag{92b}$$

The appearance of a three-body force in the doublet channel implies the correlation of different three-body observables. The short-range EFT describes these correlations therefore with the minimal number of degrees of freedom and all observed correlation lines are therefore a consequence of the large scattering length in the two-nucleon system. The short-range EFT also offers a different perspective on the internucleon interaction: different two-nucleon interactions may describe two-body data equally well but give different predictions for three-body observables.

Finite Range Corrections:

Since the ratio of effective range over scattering length in the spin-triplet channel is approximately $R/a \sim 1/3$, the consistent calculation of finite range corrections is crucial for an accurate description of low-energy observables in nuclear physics. In the three-nucleon context, range corrections were first addressed by Hammer and Mehen [26]. They included the the first subleading correction perturbatively. Bedaque *et al.* [30] calculated finite range corrections up N2LO in the EFT expansion using the modified version of the STM equation discussed in subsection 2.3. They calculated phase shifts for neutron-deuteron scattering up to N2LO using the triton binding energy and the neutron-deuteron scattering length as three-body input parameters. In [33] the powercounting results from Ref. [32] were used to calculate scattering phase shifts for S -wave scattering in the neutron-deuteron doublet channel up to N2LO. The triton binding energy was calculated as a function of the neutron-deuteron scattering length a_3 . In

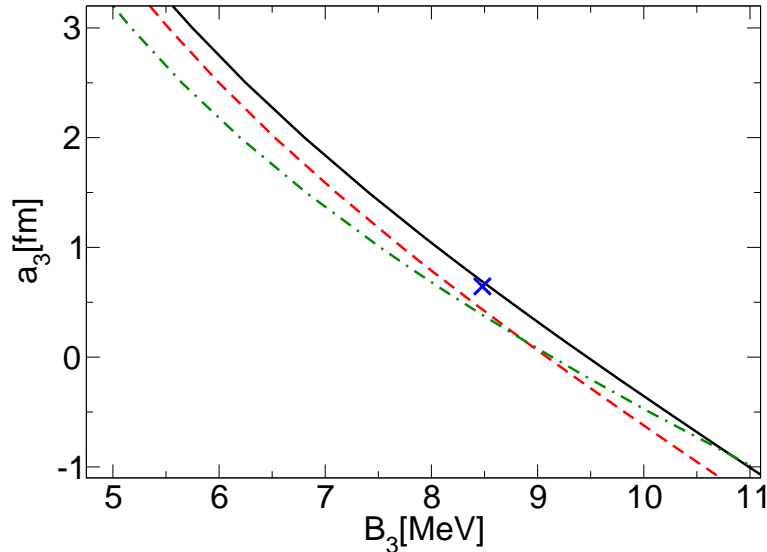


Figure 13. The Phillips line for leading (dot-dashed line), next-to-leading (dashed line) and next-to-next-to-leading (solid line) order. The cross denotes the experimental value.

Fig. 13 we show the result for this correlation line (the Phillips line). The dot-dashed, dashed and solid line show the LO, NLO and N2LO results, respectively. The cross denotes the experiment result for the triton binding energy and the neutron-deuteron scattering length. The lines in Fig. 13 are not parallel to each other since the shift from order to order depends on two expansion parameters, κr_s and γr_s (with $\kappa = \sqrt{mB_t}$). At the experimental value of the nd scattering length we find for the triton binding energy

$$B_t = (8.08(\text{LO}) + 0.11(\text{NLO}) + 0.35(\text{N2LO})) \text{ MeV} . \quad (93)$$

These 8.54 MeV are in very good agreement with the experimental value $B_t^{\text{exp}} = 8.48 \text{ MeV}$ and within the naively expected error bounds of a N2LO calculations. These results furthermore exemplify the unusual convergence pattern of the short-range EFT for three-body observables. This is due to the unnaturally small NLO correction while the N2LO corrections has the size as predicted by naive dimensional analysis. We explained in Section 2.3 that in the unitary limit the discrete scale invariance of the LO wave function prohibits the bound state spectrum to obtain any NLO correction in the unitary limit. It is tempting to speculate that the approximate discrete scale invariance of the leading order amplitude at unitarity is also partially responsible for the unexpected convergence pattern in the three-nucleon sector.

Electroweak Observables:

A major benefit of using a field-theoretic framework is the straightforward inclusion of external currents. The short-range EFT facilitates therefore the calculation of electroweak observables of few-nucleon reactions. This is particularly useful since a number of reactions relevant to nuclear astrophysics occur at energies well below the breakdown scale of the short-range EFT which is set by

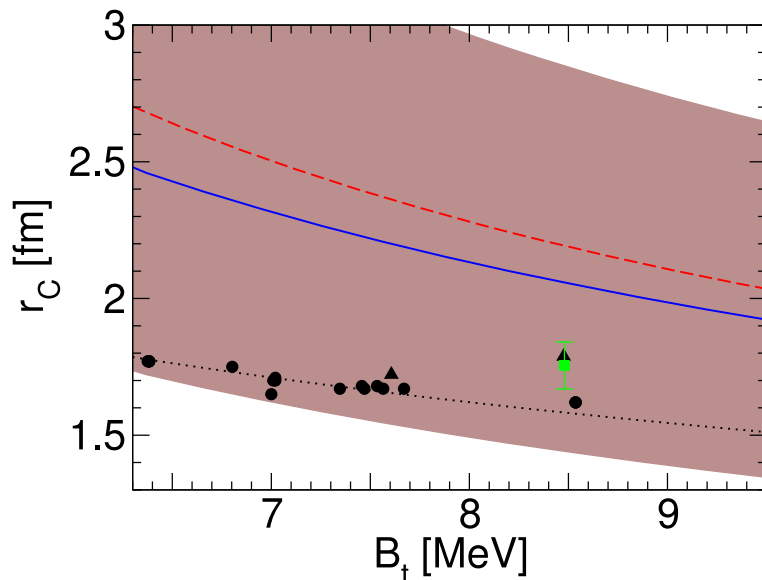


Figure 14. The correlation between the triton charge radius and binding energy. The solid (dashed) line denotes the leading-order result using a_t and a_s (B_d and a_s) as input parameters. The circles indicate Faddeev calculations using different potentials from Ref. [87] while the square gives the experimental values.

the pion mass. The number of three-body calculations with external currents is however, extremely limited. Universal properties of the electric form factor and charge radius of the triton were considered in [84]. The leading order wave function was used to evaluate the charge form factor from the leading order charge operator

$$F_C(\mathbf{q}^2) = \langle \Psi_{\mathbf{K}+\mathbf{q}} | \rho_C | \mathbf{k}_i \Psi_{\mathbf{K}} \rangle, \quad (94)$$

where $\mathbf{q} = \mathbf{k}_i - \mathbf{k}_f$, \mathbf{k}_i and \mathbf{k}_f are the initial and final momentum of the scattered electron, and $\Psi_{\mathbf{K}}$ denotes the full triton wave function with center of mass momentum \mathbf{K} . The charge density operator ρ_C is defined as [85]

$$\rho_C = \sum_i^3 \left[\frac{1}{2} (1 + \tau_{iz}) \rho_C^p(\mathbf{r} - \mathbf{r}_i) + \frac{1}{2} (1 - \tau_{iz}) \rho_C^n(\mathbf{r} - \mathbf{r}_i) \right]. \quad (95)$$

The charge radius $\langle r^2 \rangle$ can then be defined as

$$F_C(\mathbf{q}^2) = 1 - \mathbf{q}^2 \langle r^2 \rangle / 6 + \dots. \quad (96)$$

In Fig. 14 we display the one-parameter correlation between the charge radius and the triton binding energy. The two lines shown in this figure correspond to two different inputs for the two-body triplet scattering length. The shaded band gives the expected error of a leading order calculation. The existence of this correlation was (to our knowledge) first pointed out in Ref. [86].

A process relevant to big bang nucleosynthesis is thermal proton capture ($p+d \rightarrow {}^3\text{He}+\gamma$). The calculation of this amplitude is complicated by the presence

of Coulomb effects. Yet, a first step towards the goal of calculating such processes within the short-range EFT framework was performed in [88, 89]. In this work the authors considered thermal neutron capture ($n + d \rightarrow {}^3\text{H} + \gamma$) and calculated the total cross section at zero energy up to N2LO. The calculation of cross sections for this process is easier since no Coulomb effects need to be considered in this reaction. The final result is

$$\begin{aligned}\sigma_{\text{tot}} &= [0.485(\text{LO}) + 0.011(\text{NLO}) + 0.007(\text{N2LO})] \text{ mb} \\ &= [0.503 \pm 0.003] \text{ mb} ,\end{aligned}\tag{97}$$

where the remaining uncertainty is an estimate of higher order effects. This theoretical result is in excellent agreement with the experiment value $\sigma_{\text{tot}}^{\text{Exp}} = 0.508 \pm 0.015 \text{ mB}$.

A first calculation of Coulomb effects in proton-deuteron scattering (in the quartet channel) was done in [90]. However, the energies relevant to big bang nucleosynthesis are significantly lower than considered in this publication and still a challenge.

4.3 Four and more Nucleons

The short-range EFT has also been applied to the four-nucleon sector [91]. The binding energy of the α -particle was calculated using the same approach as discussed in subsection 2.4. In the case of the nuclear system, two effective potentials have to be introduced:

$$V_s = \lambda_s \mathcal{P}_s |g\rangle \langle g| ,\tag{98}$$

$$V_t = \lambda_t \mathcal{P}_t |g\rangle \langle g| ,\tag{99}$$

where V_s (V_t) denotes the spin-singlet (triplet) potential. \mathcal{P}_s and \mathcal{P}_t projects on the spin-singlet and triplet channels, respectively. The coupling constants λ_s and λ_t are therefore renormalized to the singlet and triplet scattering lengths. The effective three-body potential is

$$V_3 = \lambda_3 \mathcal{P}_A |\xi\rangle \langle \xi| ,\tag{100}$$

where \mathcal{P}_A is the operator that projects on the completely antisymmetrized three-nucleon state. The three-body coupling constant λ_3 can be adjusted using the triton binding energy.

The correlation line between triton and the α particle binding energy were calculated using the Faddeev and Faddeev-Yakubovskii equations. In Fig. 15 we show this correlation which is also known as the Tjon line. Since the short-range EFT uses the minimal number of degrees of freedom for the construction of the interaction, it explains therefore the old observation of the linear correlation between B_t and B_α . In Fig. 15 we show for example also calculations using phenomenological potentials [92] and a chiral EFT potential with explicit pions [93, 94]. All these calculations have to lie in the band generated with the short-range EFT since these potentials reproduce the large scattering length of the internucleon interaction. By the same logic, the short-range EFT also explains

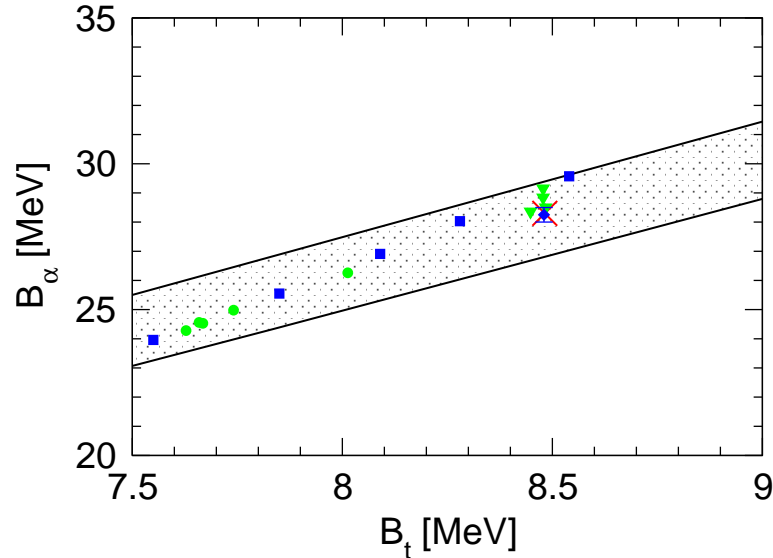


Figure 15. The correlation between triton and alpha particle binding energies, as predicted by the short-range EFT. The grey circles and triangles show various calculations using phenomenological potentials [92]. The squares show the results of chiral EFT at NLO for different cutoffs while the diamond gives the N²LO result [93, 94]. The cross shows the experimental point.

why different versions of the renormalization group evolved potential $V_{\text{low } k}$ reproduce the Tjon line [97].

The short-range EFT was also used to calculate the properties of heavier systems than the α -particle. Stetcu *et al.* [98] considered the α -particle and ${}^6\text{Li}$ using the short-range EFT in combination with the no-core shell model. They reproduced the ground-state results for the α -particle and gave an estimate for the binding energy of its first excited 0^+ state. The agreement with the experimental value of the ${}^6\text{Li}$ ground state was at the 70 % level.

4.4 Halo Nuclei

Another exciting arena for the short-range EFT is the physics of halo nuclei. Halo nuclei are weakly bound systems which consist of a tightly bound core and a “halo” of one or more nucleons. The radius of a halo nucleus is typically much larger than the radius of the core since the total binding energy of such a system is comparable to the binding energy of its core. A well-known example is ${}^6\text{He}$, a system consisting of an α -particle core and two neutrons.

Over the last years ab-initio, wave functions methods (that start from a realistic internucleon interaction) have made considerable progress in describing the lighter of the known halo systems [99], however calculations for heavier systems such as ${}^{11}\text{Li}$ or ${}^{20}\text{C}$ are not under control yet. The short-range EFT offers an alternative perspective on these systems by treating the core of the halo as a separate degree of freedom. A system such as ${}^6\text{He}$ becomes therefore an effective three-body problem and its properties can be calculated with the methods

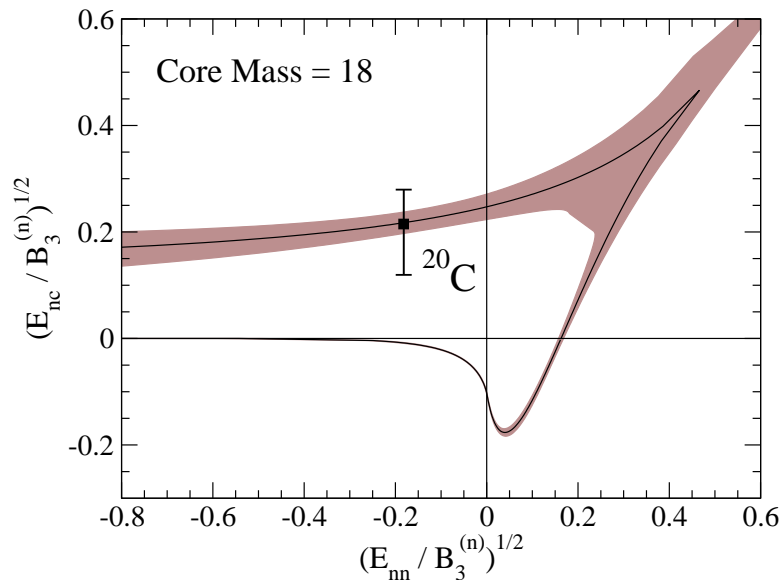


Figure 16. Boundary curve in the $\sqrt{E_{nc}/B_3^{(n)}}$ vs. $\sqrt{E_{nn}/B_3^{(n)}}$ plane with leading order error bands. Boundary curve shown for a core mass of $A = 18$ with the experimental data for ^{20}C from Ref. [104].

discussed in the previous sections. Such an approach is interesting for several reasons. It allows to test whether these systems have features related to large scattering length physics such as excited Efimov states but provides also testable predictions for observables such matter and charge radii. A further advantage of this approach is that scattering observables become directly accessible and can be calculated without any further approximations.

The first application of the short-range EFT to halo nuclei was carried out in Refs. [100, 101]. In these works the authors considered the one-neutron halo ^5He and calculated in particular phase shifts and cross sections for elastic α -nucleon scattering. A further example of a nuclear two-body cluster that has been considered is the $2\text{-}\alpha$ system [102].

Recently, Canham and Hammer [103] performed the first EFT calculation for two-neutron halos. In their work they calculated the binding energies and radii of halos such ^{11}Li and ^{20}C . Canham and Hammer also addressed the question whether any of the considered systems supports an excited Efimov state. Fig. 16 shows a parametric plot $((E_{nc}/B_3^{(n)})^{1/2}$ versus $(E_{nn}/B_3^{(n)})^{1/2}$) which describes the region in the two-body parameter space that supports a three-body state above $B_3^{(n)}$. They found that the ^{20}C system might exhibit an excited Efimov state close to the threshold. The ^6He halo nucleus was not considered by Canham and Hammer since it is expected to have P -wave resonance in the neutron-core subsystem. This feature raises also the question whether a three-body force is required for consistent renormalization in this system. A successful description of the effective three-body system would furthermore lead to the exciting problem of describing ^8He (the effective five-body problem) within the short-range EFT.

4.5 Challenges and Opportunities II

Currently, calculations for observables have only been performed up to N2LO in the EFT expansion. A computation up to N3LO would provide further information on the convergence radius of the short-range EFT. This is also required to fulfill the original promise of outstanding accuracy for few-body observables in the few-nucleon sector.

The inclusion of Coulomb effects has also to be addressed in the near future. It is known in the two-body case how to calculate the scattering of, for example, two protons. This problem has not been solved to full satisfaction in the three-body case although it is crucial for the calculation of scattering processes relevant to nuclear astrophysics such $pd \rightarrow {}^3\text{He} \gamma$. Progress in this direction is also required for further applications of the short-range EFT in the four-nucleon sector such as a calculation of the cross sections for the processes commonly denoted as HEP (${}^3\text{He}+p \rightarrow {}^4\text{He}+e^+ + \nu_e$) and HEN (${}^3\text{He}+n \rightarrow {}^4\text{He}+\gamma$).

The calculation of such four-body processes will furthermore require the development of numerical tools which facilitate the calculation of the corresponding scattering amplitudes³. With such tools at hand, the existence of further universal correlation lines could be explored (e.g. the correlation between nucleon-triton scattering length and binding energy as presented for example in [106]).

5 Final Words

We have demonstrated that the short-range EFT is an excellent tool to analyze the properties of systems whose constituents exhibit a large two-body scattering length.

Atomic physics provides a good testing ground and gives additional justification to analyze the more general (scattering length dependent) implications for such systems. It furthermore gives challenges to find solutions to problems that are not encountered in the nuclear physics case such as, for example, deeply bound two-body states that need to be accounted for in a sound manner.

The short-range EFT has also provided an alternative perspective on the topic of three-body forces. The importance of three-body forces depends strongly on the resolution at short distances of the chosen approach. In EFT approaches to nuclear systems that employ pionic degrees of freedom, the first three-body forces are generally required at higher orders in the EFT expansion. There is therefore nothing fundamental about a three-body force, but it is rather a further necessary tool to account for unknown short-distance physics.

It has also been shown that pionic degrees of freedom are irrelevant to the description of a number of important quantities such as the triton bound state or the α -particle. A number of observables have been computed beyond leading order and excellent agreement with experiment and/or calculations using realistic internucleon was found.

We have tried to supply a number of open problems that should be addressed in the near future. We hope they are understood not as barriers but as excep-

³While this manuscript was finalized we became aware of a first calculation of four-nucleon scattering observables using the framework of the short-range EFT [105].

tional chances for the short-range EFT to largely extend its current region of applicability.

Acknowledgement. I thank Eric Braaten, Hans-Werner Hammer and Daniel Phillips for useful discussions and valuable comments on this manuscript. This work was supported in part by the National Science Foundation under Grant No. PHY-0653312, and the UNEDF SciDAC Collaboration under DOE Grant DE-FC02-07ER41457.

References

1. V. Efimov, Phys. Lett. **33B**, 563 (1970).
2. E. Braaten and H. W. Hammer, Phys. Rept. **428**, 259 (2006) [arXiv:cond-mat/0410417].
3. E. Braaten and H. W. Hammer, Annals Phys. **322**, 120 (2007) [arXiv:cond-mat/0612123].
4. P. F. Bedaque and U. van Kolck, Ann. Rev. Nucl. Part. Sci. **52**, 339 (2002) [arXiv:nucl-th/0203055].
5. E. Epelbaum, H. W. Hammer and U. G. Meißner, arXiv:0811.1338 [nucl-th].
6. D. B. Kaplan, arXiv:nucl-th/0510023.
7. G. P. Lepage, arXiv:nucl-th/9706029.
8. J. Polchinski, arXiv:hep-th/9210046.
9. D. R. Phillips, Czech. J. Phys. **52**, B49 (2002) [arXiv:nucl-th/0203040].
10. U. van Kolck, Nucl. Phys. A **645**, 273 (1999) [arXiv:nucl-th/9808007].
11. D. B. Kaplan, M. J. Savage and M. B. Wise, Phys. Lett. B **424**, 390 (1998) [arXiv:nucl-th/9801034].
12. D. B. Kaplan, M. J. Savage and M. B. Wise, Nucl. Phys. B **534**, 329 (1998) [arXiv:nucl-th/9802075].
13. J. Gegelia, Phys. Lett. B **429**, 227 (1998).
14. M. C. Birse, J. A. McGovern and K. G. Richardson, PiN Newslett. **15**, 280 (1999) [arXiv:nucl-th/9911048].
15. H. W. Hammer and R. J. Furnstahl, Nucl. Phys. A **678**, 277 (2000) [arXiv:nucl-th/0004043].
16. L. Platter, H. W. Hammer and U.-G. Meißner, Nucl. Phys. A **714**, 250 (2003) [arXiv:nucl-th/0208057].
17. P. F. Bedaque, H. W. Hammer and U. van Kolck, Phys. Rev. Lett. **82**, 463 (1999) [arXiv:nucl-th/9809025].

18. P. F. Bedaque, H. W. Hammer and U. van Kolck, Nucl. Phys. A **646**, 444 (1999) [arXiv:nucl-th/9811046].
19. G.V. Skorniakov and K.A. Ter-Martirosian, Sov. Phys. JETP **4**, 648 (1957).
20. G.S. Danilov, Sov. Phys. JETP **13**, 349 (1961) [J. Exptl. Theoret. Phys. (U.S.S.R.) **40**, 498 (1961)].
21. V.F. Kharchenko, Sov. J. Nucl. Phys. **16**, 173 (1973) [Yad. Fiz. **16**, 310 (1972)].
22. E. Nielsen, D.V. Fedorov, A.S. Jensen, and E. Garrido, Phys. Rep. **347**, 373 (2001).
23. K. G. Wilson, Phys. Rev. D **3**, 1818 (1971).
24. V. Efimov, Phys. Rev. C **44**, 2303 (1991).
25. V. Efimov, Phys. Rev. C **47**, 1876 (1993).
26. H. W. Hammer and T. Mehen, Phys. Lett. B **516**, 353 (2001) [arXiv:nucl-th/0105072].
27. L. Platter, C. Ji and D. R. Phillips, arXiv:0808.1230 [cond-mat.other].
28. M. Thøgersen, D. V. Fedorov and A. S. Jensen, Phys. Rev. A **78**, 020501 (2008).
29. C. Ji, D. R. Phillips and L. Platter, *in progress*.
30. P. F. Bedaque, G. Rupak, H. W. Griesshammer and H. W. Hammer, Nucl. Phys. A **714**, 589 (2003) [arXiv:nucl-th/0207034].
31. F. Gabbiani, arXiv:nucl-th/0104088.
32. L. Platter and D. R. Phillips, Few Body Syst. **40**, 35 (2006) [arXiv:cond-mat/0604255].
33. L. Platter, Phys. Rev. C **74**, 037001 (2006) [arXiv:nucl-th/0606006].
34. H. W. Hammer, D. R. Phillips and L. Platter, Eur. Phys. J. A **32**, 335 (2007) [arXiv:0704.3726 [nucl-th]].
35. H. W. Griesshammer, Nucl. Phys. A **760**, 110 (2005) [arXiv:nucl-th/0502039].
36. L. Platter, H. W. Hammer and U. G. Meißner, Phys. Rev. A **70**, 052101 (2004) [arXiv:cond-mat/0404313].
37. W. Glöckle, *The Quantum Mechanical Few-Body Problem*, (Springer, 1983).
38. E.W. Schmid and H. Ziegelmann, *The Quantum Mechanical Three-Body Problem*, (Vieweg, 1971).

39. H. W. Hammer and L. Platter, *Eur. Phys. J. A* **32**, 113 (2007) [arXiv:nucl-th/0610105].
40. W. Schöllkopf and J.P. Toennies, *J. Chem. Phys.* **104**, 1155 (1996).
41. V. Roudnev and S. Yakovlev, *Chem. Phys. Lett.* **328**, 97 (2000).
42. V. Roudnev, *Chem. Phys. Lett.* **367**,95 (2003).
43. A.K. Motovilov, W. Sandhas, S.A. Sofianos, and E.A. Kolganova, *Eur. Phys. J. D* **13**, 33 (2001).
44. Kolganova, E. A., Motovilov, A. K., Sandhas, W.: *Phys. Rev. A* **70**, 052711 (2004)
45. D. Blume and C.H. Greene, *J. Chem. Phys.* **112**, 8053 (2000).
46. M. Lewerenz, *J. Chem. Phys.* **106**, 4596 (1997).
47. S. Nakaichi-Maeda and T.K. Lim, *Phys. Rev. A* **28**, 692 (1983).
48. J. von Stecher, J. P. DIncao, and C. H. Greene, arXiv:0810.3876.
49. T. Kraemer, M. Mark, P. Waldburger, J.G. Danzl, C. Chin, B. Engeser, A. D. Lange, K. Pilch, A. Jaakkola, H.-C. Nägerl, and R. Grimm, *Nature* **440**, 315 (2006).
50. T. B. Ottenstein, T. Lompe, M. Kohnen, A. N. Wenz, and S. Jochim, arXiv:0806.0587.
51. J. H. Huckans, J. R. Williams, E. L. Hazlett, R. W. Stites, and K. M. O'Hara, arXiv:0810.3288.
52. M. Zaccanti, G. Modugno, C. D'Erico, M. Farroti, G. Roati, and M. Inguscio, talk at DAMOP 2008, State College, Pennsylvania, USA.
53. G. Thalhammer, G. Barontini, J. Catani, F. Rabatti, C. Weber, A. Simoni, F. Minardi and M. Inguscio, arXiv:0903.0976.
54. F. Ferlaino, S. Knoop, M. Berninger, W. Harm, J. P. D'Incao, H.-C. Nägerl, R. Grimm, arXiv:0903.1276.
55. P. F. Bedaque, E. Braaten and H. W. Hammer, *Phys. Rev. Lett.* **85**, 908 (2000) [arXiv:cond-mat/0002365].
56. B. D. Esry, C. H. Greene, and H. Suno, *Phys. Rev. A* **65**, 010705 (2001).
57. J. H. Macek, S. Ovchinnikov, and G. Gasaneo, *Phys. Rev. A* **72**, 032709 (2005).
58. J. H. Macek, S. Ovchinnikov, and G. Gasaneo, *Phys. Rev. A* **73**, 032704 (2006).

59. D. Petrov, talk at the Workshop on Strongly Interacting Quantum Gases, Ohio State University, April 2005.
60. E. Nielsen and J. H. Macek, Phys. Rev. Lett. **83**, 1566 (1999).
61. B. D. Esry, C. H. Greene, and J. P. Burke, Phys. Rev. Lett. **83**, 1751 (1999).
62. E. Braaten and H. W. Hammer, Phys. Rev. A **70**, 042706 (2004) [arXiv:cond-mat/0303249].
63. E. Braaten and H. W. Hammer, Phys. Rev. Lett. **87**, 160407 (2001) [arXiv:cond-mat/0103331].
64. V. Efimov, Sov. J. Nucl. Phys. **29**, 546 (1979) [Yad. Fiz. **29**, 1058 (1979)].
65. E. Braaten, H. W. Hammer, D. Kang and L. Platter, Phys. Rev. A **78**, 043605 (2008) [arXiv:0801.1732 [cond-mat.other]].
66. H. W. Hammer, T. A. Lahde and L. Platter, Phys. Rev. A **75**, 032715 (2007) [arXiv:cond-mat/0611769].
67. E. Braaten, H. W. Hammer, D. Kang and L. Platter, arXiv:0811.3578 [cond-mat.other].
68. P. Naidon and M Ueada, arXiv:0811.4086.
69. R. Schmidt, S. Floerchinger and C. Wetterich, arXiv:0812.1191.
70. E. Braaten and H. W. Hammer, Phys. Rev. A **75**, 052710 (2007) [arXiv:cond-mat/0610116].
71. K. Helfrich and H. W. Hammer, arXiv:0902.3410 [cond-mat.other].
72. S. Knoop et al., arXiv:0807.3306 [cond-mat].
73. J. von Stecher, J. P. DIncao, and C. H. Greene, arXiv:0903.3348 (2009).
74. E. Epelbaum, Prog. Part. Nucl. Phys. **57**, 654 (2006) [arXiv:nucl-th/0509032].
75. S. Christlmeier and H. W. Griesshammer, Phys. Rev. C **77**, 064001 (2008) [arXiv:0803.1307 [nucl-th]].
76. H. Arenhövel, W. Leidemann and E. L. Tomusiak, Eur. Phys. J. A **23** (2005) 147 [arXiv:nucl-th/0407053].
77. T. Tamae et al., Phys. Rev. Lett. **59** (1987) 2919.
78. P. von Neumann-Cosel et al., Phys. Rev. Lett. **88** (2002) 202304.
79. N. Ryezayeva *et al.*, Phys. Rev. Lett. **100**, 172501 (2008).
80. S. I. Ando, Eur. Phys. J. A **33**, 185 (2007) [arXiv:0707.2157 [nucl-th]].

81. D. R. Phillips, M. R. Schindler and R. P. Springer, arXiv:0812.2073 [nucl-th].
82. P. F. Bedaque, H. W. Hammer and U. van Kolck, Phys. Rev. C **58**, 641 (1998) [arXiv:nucl-th/9802057].
83. P. F. Bedaque, H. W. Hammer and U. van Kolck, Nucl. Phys. A **676**, 357 (2000) [arXiv:nucl-th/9906032].
84. L. Platter and H. W. Hammer, Nucl. Phys. A **766**, 132 (2006) [arXiv:nucl-th/0509045].
85. J.L. Friar, B.F. Gibson, E.L. Tomusiak, and G.L. Payne, Phys. Rev. C **24**, 665 (1981).
86. J.L. Friar, B.F. Gibson, C.R. Chen, and G.L. Payne, Phys. Lett. **161B**, 241 (1985).
87. C.R. Chen, G.L. Payne, J.L. Friar, and B.F. Gibson, Phys. Rev. C **31**, 2266 (1985).
88. H. Sadeghi, S. Bayegan and H. W. Griefhammer, Phys. Lett. B **643**, 263 (2006).
89. H. Sadeghi and S. Bayegan, Nucl. Phys. A **753**, 291 (2005).
- g
90. G. Rupak and X. W. Kong, Nucl. Phys. A **717**, 73 (2003) [arXiv:nucl-th/0108059].
91. L. Platter, H. W. Hammer and U. G. Meißner, Phys. Lett. B **607**, 254 (2005) [arXiv:nucl-th/0409040].
92. A. Nogga, H. Kamada and W. Glöckle, Phys. Rev. Lett. **85**, 944 (2000). [arXiv:nucl-th/0004023].
93. E. Epelbaum, H. Kamada, A. Nogga, H. Witała, W. Glöckle and U.-G. Meißner, Phys. Rev. Lett. **86**, 4787 (2001). [arXiv:nucl-th/0007057].
94. E. Epelbaum, A. Nogga, W. Glöckle, H. Kamada, U.-G. Meißner and H. Witała, Phys. Rev. C **66**, 064001 (2002). [arXiv:nucl-th/0208023].
95. D.H. Beck et al., Phys. Rev. C **30**, 1403 (1984).
96. D. Beck et al., Phys. Rev. Lett. **59**, 1537 (1987).
97. A. Nogga, S. K. Bogner and A. Schwenk, Phys. Rev. C **70**, 061002 (2004) [arXiv:nucl-th/0405016].
98. I. Stetcu, B. R. Barrett and U. van Kolck, Phys. Lett. B **653**, 358 (2007) [arXiv:nucl-th/0609023].
99. S. Bacca, A. Schwenk, G. Hagen and T. Papenbrock, arXiv:0902.1696 [nucl-th].

100. C. A. Bertulani, H. W. Hammer and U. Van Kolck, Nucl. Phys. A **712**, 37 (2002) [arXiv:nucl-th/0205063].
101. P. F. Bedaque, H. W. Hammer and U. van Kolck, Phys. Lett. B **569**, 159 (2003) [arXiv:nucl-th/0304007].
102. R. Higa, H. W. Hammer and U. van Kolck, Nucl. Phys. A **809**, 171 (2008) [arXiv:0802.3426 [nucl-th]].
103. D. L. Canham and H. W. Hammer, Eur. Phys. J. A **37**, 367 (2008) [arXiv:0807.3258 [nucl-th]].
104. TUNL nuclear data evaluation project, <http://www.tunl.duke.edu/NuclData/>.
105. J. Kirscher, H. W. Griesshammer, D. Shukla and H. M. Hofmann, arXiv:0903.5538 [nucl-th].
106. A. Deltuva and A. C. Fonseca, Phys. Rev. C **75**, 014005 (2007) [arXiv:nucl-th/0611029].